

The Soil Moisture Active Passive Experiments: Validation of the SMAP Products in Australia

Nan Ye¹, Jeffrey P. Walker², *Fellow, IEEE*, Xiaoling Wu³, *Member, IEEE*, Richard de Jeu, Ying Gao⁴, *Member, IEEE*, Thomas J. Jackson⁵, *Fellow, IEEE*, François Jonard⁶, *Member, IEEE*, Edward Kim, *Senior Member, IEEE*, Olivier Merlin, Valentijn R. N. Pauwels⁷, Luigi J. Renzullo, *Member, IEEE*, Christoph Rüdiger⁸, *Senior Member, IEEE*, Sabah Sabaghy, Christian von Hebel, Simon H. Yueh⁹, *Fellow, IEEE*, and Liujun Zhu

Abstract—The fourth and fifth Soil Moisture Active Passive Experiments (SMAPEX-4 and -5) were conducted at the beginning of the SMAP operational phase, May and September 2015, to: 1) evaluate the SMAP microwave observations and derived soil moisture (SM) products and 2) intercompare with the Soil Moisture and Ocean Salinity (SMOS) and Aquarius missions over the Murrumbidgee River Catchment in the southeast of Australia. Airborne radar and radiometer observations at the same microwave frequencies as SMAP were collected over SMAP footprints/grids concurrent with its overpass. In addition, intensive ground sampling of SM, vegetation water content, and surface roughness was carried out, primarily for validation of airborne SM retrieval over six $\sim 3 \text{ km} \times 3 \text{ km}$ focus areas. In this study, the SMAPEX-4 and -5 data sets were used as independent reference for extensively evaluating the brightness temperature and SM products of SMAP, and intercompared with SMOS and Aquarius under a wide range of SM and vegetation conditions. Importantly, this is the only extensive airborne field campaign that collected data while the SMAP radar was still operational. The SMAP radar, radiometer, and derived SM showed a high agreement with the SMAPEX-4 and -5 data set,

with a root-mean-squared error (RMSE) of $\sim 3 \text{ K}$ for radiometer brightness temperature, and an RMSE of $\sim 0.05 \text{ m}^3/\text{m}^3$ for the radiometer-only SM product. The SMAP radar backscatter had an RMSE of 3.4 dB, while the retrieved SM had an RMSE of $0.11 \text{ m}^3/\text{m}^3$ when compared with the SMAPEX-4 data set.

Index Terms—Calibration and validation, field experiment, passive microwave remote sensing, radar remote sensing, remote sensing, soil moisture (SM).

I. INTRODUCTION

SOIL moisture (SM) is a crucial variable at the interface between the atmosphere and the land surface, controlling the partitioning of rainfall into runoff [1], evapotranspiration [2], and microorganism activity [3]. Its spatial distribution and temporal evolution are required in many disciplines including hydrology, meteorology, and agriculture [4]–[6]. However, SM is difficult to measure or predict at regional and global scales, due to its high variability in space and time. In recent decades, microwave radiometry at the L-band (1–2 GHz) has been widely acknowledged as the most promising technique for monitoring near surface SM, due to its all-weather capability, direct relation to volumetric SM through the soil dielectric constant, and reduced attenuation and scattering effects from the vegetation canopy and surface roughness [7], [8]. Consequently, the first two space missions dedicated to SM measurement have both employed L-band (1.41 GHz) radiometers to measure the soil water content in the top $\sim 5 \text{ cm}$ soil layer every 2–3 days, with a target accuracy of better than $0.04 \text{ m}^3/\text{m}^3$ [9], [10]. The L-band radiometry technique is also being considered in future mission plans including the Water Cycle Observation Mission (WCOM) [11] and the Terrestrial Water Resources Satellite (TWRS) [12].

The Soil Moisture and Ocean Salinity (SMOS) mission was developed by the European Space Agency (ESA) and launched on November 2, 2009. However, since the SMOS SM data have a spatial resolution of $\sim 40 \text{ km}$, its use has been limited in hydroclimatology applications [9]. The Soil Moisture Active and Passive (SMAP) mission was launched by the National Aeronautics and Space Administration (NASA) on January 31, 2015, carrying an L-band (1.26 GHz) radar in addition to the radiometer to enable SM retrieval at an intermediate spatial

Manuscript received April 11, 2020; revised June 11, 2020; accepted June 16, 2020. This work was supported by the Australian Research Council through the Moisture Monitor Project under Grant DP140100572. (Corresponding author: Nan Ye.)

Nan Ye, Jeffrey P. Walker, Xiaoling Wu, Ying Gao, Valentijn R. N. Pauwels, Christoph Rüdiger, Sabah Sabaghy, and Liujun Zhu are with the Department of Civil Engineering, Monash University, Clayton, VIC 3800, Australia (e-mail: nan.ye@monash.edu).

Richard de Jeu is with Transmissivity B.V., Space Technology Center, 2201 DK Noordwijk, The Netherlands.

Thomas J. Jackson, retired, is with USDA-ARS, Hydrology and Remote Sensing Laboratory, Beltsville, MD 20705 USA.

François Jonard is with Earth and Life Institute, Université catholique de Louvain, 1348 Louvain-la-Neuve, Belgium, and also with the Institute of Bio- and Geosciences—Agrosphere (IBG-3), Forschungszentrum Jülich GmbH, 52428 Jülich, Germany.

Edward Kim is with NASA Goddard Space Flight Center, Greenbelt, MD 20771 USA.

Olivier Merlin is with CESBIO, Université de Toulouse, IRD/UPS/CNRS/CNES, 31400 Toulouse, France.

Luigi J. Renzullo is with the Fenner School of Environment and Society, The Australian National University, Canberra, ACT 0200, Australia.

Christian von Hebel is with the Institute of Bio- and Geosciences—Agrosphere (IBG-3), Forschungszentrum Jülich GmbH, 52428 Jülich, Germany.

Simon H. Yueh is with NASA Jet Propulsion Laboratory, Pasadena, CA 91109 USA.

Color versions of one or more of the figures in this article are available online at <http://ieeexplore.ieee.org>.

Digital Object Identifier 10.1109/TGRS.2020.3007371

resolution of ~ 9 km, using the high-resolution backscatter observations for downscaling so as to meet the spatial resolution requirement of hydrometeorology and agriculture applications [10]. This innovative approach was demonstrated prior to the launch of SMAP using combined airborne L-band radar and radiometer sensors across a number of field experiments, such as the Soil Moisture Experiments [SMEX; 13, 14], the Cloud and Land Surface Interaction Campaign (CLASIC) [15], the SMAP Validation Experiments (SMAPVEX) [16], and the SMAPEX-1 to -3 [17].

Since SM can be derived from either radar or radiometer technology, the SMAP mission was designed to provide three types of SM products: 1) radiometer-only at 36 km; 2) radar-only at 3 km; and 3) radar-radiometer at 9 km. In addition to SMOS and SMAP, Aquarius also carried an L-band radiometer and radar. Though designed primarily for monitoring global ocean salinity [18], it has also been used to retrieve SM [19]. The Aquarius radar and radiometer launched by NASA on June 10, 2011 had three beams with incidence angles of 28.7° , 37.8° , and 45.6° , with spatial resolutions of 94, 120, and 156 km, respectively [18]. Due to different life times of SMAP, SMOS, and Aquarius, it is important to evaluate the consistency of brightness temperature and derived SM between the different space-borne L-band radiometers, to explore the possibility of merging the three observational data sets for deriving a long-term consistent and harmonized record, critical for flood forecasting, numerical weather prediction, and drought monitoring and prediction [20].

The Soil Moisture Active Passive Experiments (SMAPEX) comprised a series of five airborne field campaigns in different seasons across a six year time frame (2010–2015), aimed at prelaunch algorithm development, and postlaunch calibration and validation of SMAP under Australian land surface conditions. The first three experiments [SMAPEX-1 to -3; 17] were carried out to support SMAP prelaunch SM retrieval and downscaling development during July 2010–September 2011. The SMAPEX-4 and -5 were conducted at the beginning of the SMAP operational phase in May and September 2015, to provide extensive airborne active and passive microwave observations, ground sampling of SM, and ancillary data coincident with SMAP coverage, with the objective to assess the SMAP in-orbit performance. As a complement to field experiments in North America, the SMAPEX-4 and -5 data sets have made an important contribution to SMAP postlaunch calibration and validation under Australian vegetation and soil conditions. The SMAPEX data set can also support algorithm developments for new satellite opportunities, such as the WCOM and TWRS missions.

Due to the failure of Aquarius and the SMAP radar in June and July 2015, respectively, SMAPEX-4 provides a unique data set to: 1) evaluate SMAP radar backscatter and SM observations; 2) evaluate SMAP Active/Passive downscaling algorithms; and 3) intercompare radiometer observations and SM products among SMAP, SMOS, and Aquarius. Consequently, this article presents the details of the SMAPEX-4 and -5 campaigns in Section II and an evaluation of SMAP products in Section III, together with an intercomparison against SMOS and Aquarius in Section IV.

TABLE I
SPECIFICATIONS OF THE AIRBORNE INSTRUMENTS. RESOLUTIONS ARE FOR THE NOMINAL FLYING HEIGHT OF 3000 m AGL

PLMR	Polarimetric L-Band Multi-beam Radiometer
Type:	L-band microwave radiometer
Frequency:	1401 - 1425 MHz
Polarization:	H & V
Observation Mode:	Push broom
Incidence angle:	6 beams: $\pm 7^\circ$, $\pm 21.5^\circ$ and $\pm 38.5^\circ$
Beam width:	15°
Ground resolution:	1000 m
Accuracy:	< 1.4 K
PLIS	Polarimetric L-band Imaging Synthetic Aperture Radar
Type:	L-band microwave radar
Frequency:	1245 - 1275 MHz
Polarization:	HH, VV, HV & VH
Observation Mode:	SAR
Incidence angle:	2 beams: $\pm 30^\circ$
Beam width:	30°
Ground resolution:	10 m
Accuracy:	< 0.7 dB
Everest Interscience 3800ZL	
Type:	Thermal Infrared Radiometer (TIR)
Wave length:	8.0 - 14.0 μm
Observation Mode:	Push broom
Incidence angle:	6 beams: $\pm 7^\circ$, $\pm 21.5^\circ$ and $\pm 38.5^\circ$
Beam width:	15°
Ground resolution:	1000 m
Skye 1870A	
Type:	Short Wave Infrared Radiometer (SWIR)
Wave length:	4 channels: 1628 - 2216 nm
Observation Mode:	Push broom
Incidence angle:	6 beams: $\pm 7^\circ$, $\pm 21.5^\circ$ and $\pm 38.5^\circ$
Beam width:	15°
Ground resolution:	1000 m
Skye 1850A	
Type:	Visible and Near Infrared Radiometer (VNIR)
Wave length:	4 channels: 459 - 876 nm
Observation Mode:	Push broom
Incidence angle:	6 beams: $\pm 7^\circ$, $\pm 21.5^\circ$ and $\pm 38.5^\circ$
Beam width:	15°
Ground resolution:	1000 m
FLIR A65	
Type:	Thermal Infrared Camera
Wave length:	7.5 - 13 μm
Observation Mode:	Snap shot
Incidence angle:	Nadir
Beam width:	$45^\circ \times 37^\circ$
Ground resolution:	~ 4 m
DSLR	Canon EOS-1Ds Mark III Digital Single Lens Reflex
Type:	Visible (RGB) Camera
Observation Mode:	Snap shot
Incidence angle:	Nadir
Beam width:	$45^\circ \times 37^\circ$
Ground resolution:	~ 0.5 m

II. SMAPEX-4 AND -5 DATA SETS

A. Airborne Instrumentation and Calibration

The SMAPEX-4 and -5 have used the same airborne instruments as the preceding SMAPEX experiments (Table I). The primary instruments include the Polarimetric L-band Multi-beam Radiometer (PLMR) and the Polarimetric L-band Imaging Synthetic aperture radar (PLIS), which were used to simulate the SMAP radiometer and radar, respectively. With daily calibration, a high accuracy was achieved for PLMR and PLIS to ensure the quality and consistency of SMAPEX airborne brightness temperature and backscatter observations across the periods of SMAPEX-4 and -5.

The PLMR has a Noise Equivalent Delta-Temperature (NEDT) of ~ 0.7 K for an integration time of 0.5 s. An accuracy of better than ~ 1.4 K was achieved based on ground calibration data before and after each flight, using sky and temperature recorded microwave absorber box observations as cold and warm targets, respectively. The calibration was further confirmed using airborne observations collected over Lake Wyangan from a low altitude pass at the end of each flight. A floating monitoring station was installed at the center of the calibration lake for each campaign, providing surface water temperature and salinity data for estimating the water brightness temperature.

At the start and end of each campaign, the PLIS was flown over three Polarimetric Active Radar Calibrators (PARCs) set up over a homogeneous grass land for absolute calibration. During each flight, the PLIS was flown over six Passive Radar Calibrators (PRCs) located across a single swath, for co-polarization calibration at incidence angles from 15° to 45° . It was also flown over a forest target for cross-polarization calibration. During the SMAPEX-4 and -5, absolute accuracy of better than 0.7 dB was achieved for all polarizations of PLIS [21].

B. Study Area

The SMAPEX series of airborne field experiments were conducted in the approximately 80000 km² Murrumbidgee River catchment in southeastern Australia, having an elevation ranging from 50 m in the west to 2018 m in the east. Consequently, the western plains are characterized as semiarid with an average annual precipitation of 300 mm, having a cropping and grazing dominated land surface with fine textured clay to sandy soils. In contrast, the eastern half of the catchment is dominated by hilly grazing areas mixed with native forests, with a temperate climate having an annual precipitation of 1900 mm and the soils having medium to coarse texture.

Due to its significant spatial variability in topography, climate, land cover, and soils, the Murrumbidgee catchment (Fig. 1) has been equipped with an extensive SM monitoring network since 2001, specifically for SM remote sensing studies. The OzNet was first established with 18 sites across the entire catchment measuring the SM and temperature profile, rainfall, and soil suction, and later upgraded with 20 “new” sites focusing on the Yanco area and Kyeamba subcatchment in 2003 [22]. For the purpose of SMAP calibration and validation, an additional 24 SMAPEX cluster sites [17] were set up within two 9-km grid cells aligned with the initial S km Equal-Area Scalable Earth (EASE-2) grid (YA and YB target areas in Fig. 1) in 2009, measuring SM and temperature in the top 5 cm of the soil layer, specifically designed to match the L-band penetration depth. As the land use map in Fig. 1 shows, YA is dominated by flood irrigation and dry land cropping areas, while YB is dominated by grazing.

The OzNet monitoring network with its long-term data sets and detailed knowledge makes the Murrumbidgee catchment an ideal basis for airborne field experiments and as a test bed for satellite SM calibration, validation, and downscaling

studies. Consequently, the Yanco area has been selected as the core site for SMAP calibration and validation in Australia [23]–[26]. In addition to the permanent OzNet sites in the Yanco area, a temporary monitoring station was installed near the center of each 3-km focus area for the periods of SMAPEX-4 and -5 (Fig. 1), providing ancillary information for correcting the temporal variation of brightness temperature during each flight, confirming the temporal variation of SM over the ground sampling period, and for the opportunity to interpolate ground data between intensive sampling days at the same focus farms (typically 7 days apart). Specifically, temporary monitoring stations recorded SM over depths of the top 5 cm and 20–25 cm soil layers; soil temperature at the depths of 2.5, 5, 15, and 40 cm; thermal infrared radiometer-based skin temperature; leaf wetness; and rainfall accumulation at 20 min intervals. The Murrumbidgee catchment has also been the focus of a number of airborne field experiments (i.e., the National Airborne Field Experiment 2006 [NAFE’06; 27], the Australian Airborne Cal/Val Experiments for SMOS [AACES; 28], and the Soil Moisture Active Passive Experiments [SMAPEX-1 to -3; 17]). The SMAPEX-4 and -5 were conducted in the Yanco area for a larger flight domain than previous SMAPEX experiments, in order to cover at least one complete footprint of the SMAP radiometer. This also meant that a wider range of land cover types and topography features were covered.

Fig. 2 shows the time series of the mean and 25th/75th percentiles of the top 5 cm SM and daily precipitation measurements averaged across “New” sites in the Yanco area. It can be seen that heavy rainfall events occurred prior to SMAPEX-4 and -5, followed by a drying out period during the experiments. In addition, two small to medium rainfall events occurred during SMAPEX-4, providing an opportunity to investigate precipitation effects on SMAP observations, and to validate SMAP products under heterogeneous SM distribution. Consequently, the SMAPEX-4 and -5 data sets provide opportunities to validate (and intercompare) SMAP (with SMOS and Aquarius) products under a wide range of SM conditions.

C. Sampling Strategy

The SMAPEX-4 and -5 were conducted in the austral autumn from April 30th to May 23rd, and austral spring from September 6, 2015 to September 28, 2015, respectively. The specific objectives were to: 1) evaluate SMAP Active–Passive downscaled 9-km radiometer observations; 2) intercompare SMAP, SMOS, and Aquarius with airborne radiometer/radar observations; 3) validate SMAP radar-only, radiometer-only, and radar–radiometer SM retrieval algorithms using airborne SM retrieval results from field experiments and long-term SM monitoring network measurements; and 4) further develop radar-only SM retrieval algorithms. During the 3 week period of SMAPEX-4, nine flights were designed over two study areas according to the 3 dB footprints of the SMAP and Aquarius radiometers, respectively (Fig. 1). Prior to the SMAPEX-5 experiment, both the Aquarius instrument and the SMAP radar failed. Consequently, there were only eight flights over

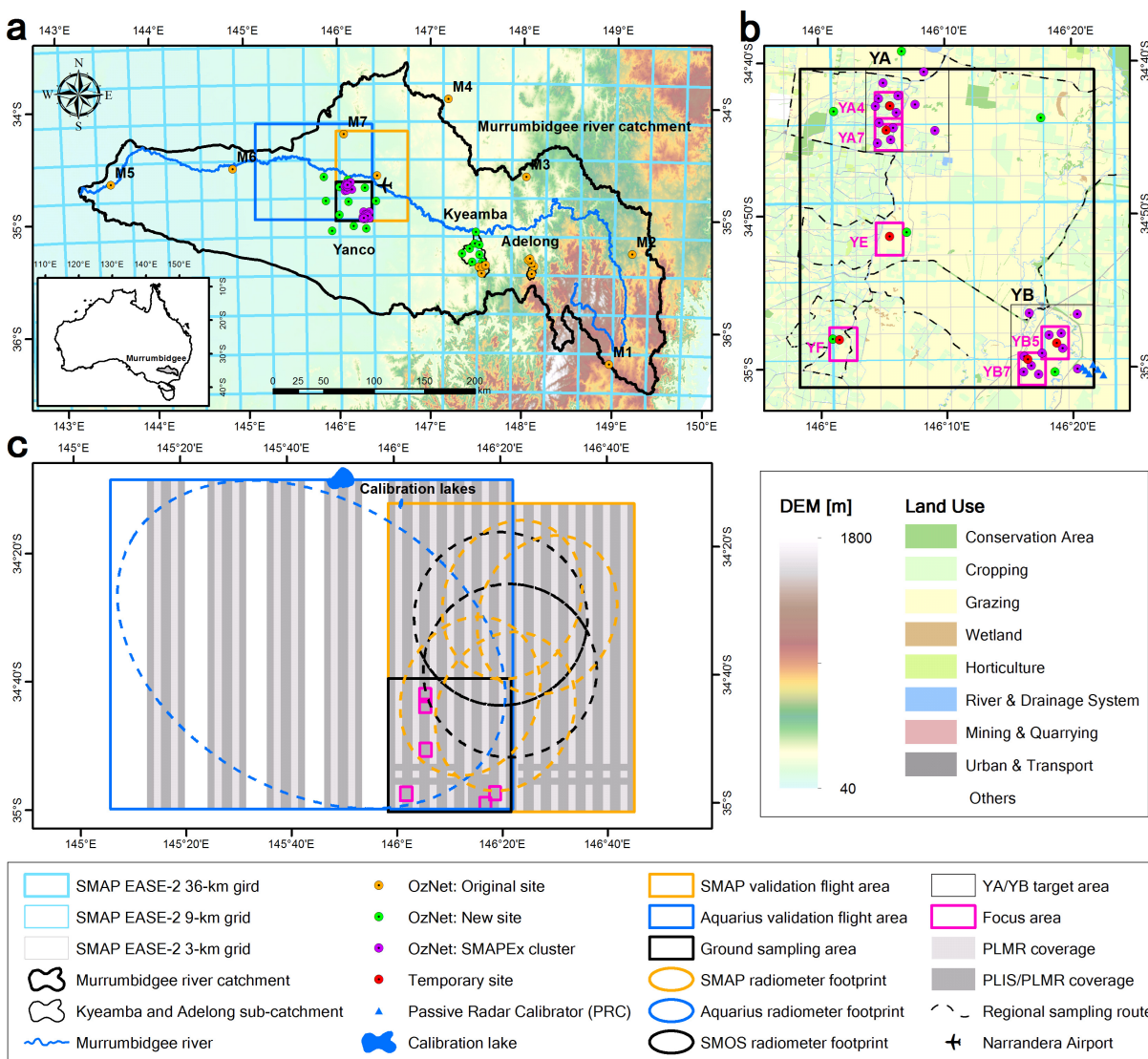


Fig. 1. (a) Location of the SMAPEX-4/-5 study area and the OzNet monitoring stations in the Murrumbidgee River Catchment with the Digital Elevation Model (DEM) and the SMAP EASE-2 grid at 36 km scale as backdrop. (b) Layout of the ground sampling focus areas and monitoring stations with land use map and the SMAP EASE-2 grids at 9 and 3 km scales as backdrop. (c) Example footprints of SMOS, SMAP, and Aquarius radiometers with coverage of airborne PLMR and PLIS observations as backdrop.

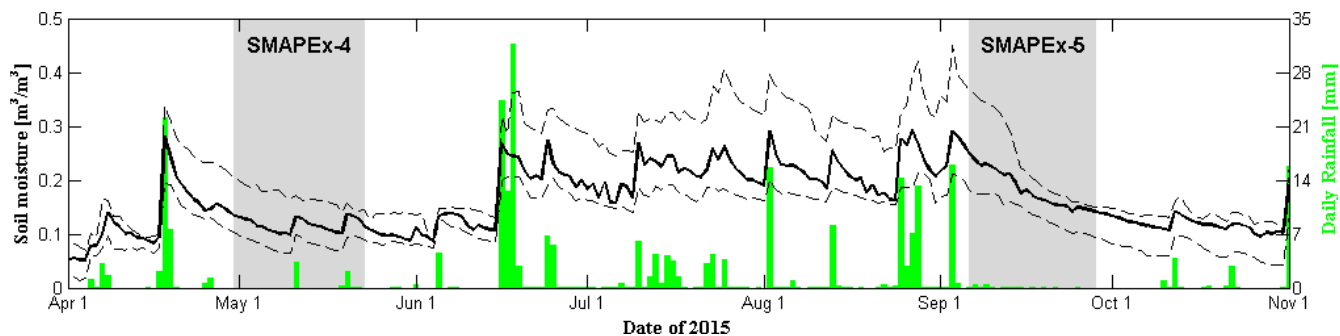


Fig. 2. Time series of the top 5 cm SM and rainfall measurements from the 11 OzNet “New” sites over the Yanco area between April 1, 2015 and November 1, 2015; the black solid lines and black dashed lines show the mean and 25th/75th percentiles of SM, respectively. The green bar shows the mean of daily rainfall recorded at the “New” sites in the Yanco area. The shaded regions show the periods of the intensive SMAPEX sampling.

the SMAP validation flight area in the second campaign. Ground sampling of the top 5 cm SM, vegetation water content (VWC), and surface roughness were collected concurrent with airborne sampling over the six 3-km focus areas (Fig. 1), in order to collect the ancillary data required for SM retrieval, and spatial SM data for validation of airborne SM retrieval.

During the preparation of SMAPEX-4, prior to the launch of SMAP, the orbit uncertainty was considered in the design of the flight areas to ensure full coverage of the SMAP radiometer footprints was attained during each SMAP overpass. SMAP utilizes a conically scanning antenna resulting in 3-dB elliptical footprints of $39 \text{ km} \times 47 \text{ km}$ with a spacing of 11 km along scans and 31 km between scans. To ensure that at least one complete SMAP footprint would be covered by the airborne instruments, a flight area of $71 \text{ km} \times 89 \text{ km}$ was identified, containing four 3 dB footprints; two adjacent along and two cross scans, from each of three nominal orbits in every 8 days repeat cycle over the Yanco area (Fig. 1). The selected SMAP validation flight area covered all of the SMAPEX cluster sites in the southwest, the topographic relief feature in the northeast, and various land surface types including urban areas and standing water bodies, which can have an adverse effect on SM retrieval accuracy [29]–[31].

For logistical reasons and to be consistent with the previous SMAPEX campaigns, regional ground sampling was restricted to the $38 \text{ km} \times 36 \text{ km}$ ground sampling area coincident with the SMAPEX-1 to -3 study area, with intensive sampling focused on six $3 \text{ km} \times 3 \text{ km}$ SMAP radar EASE-2 pixels (Fig. 1). Four of these six 3-km focus areas, including YA4 and YA7 from the YA cropping area, as well as YB5 and YB7 from the YB grazing area, have dense SM cluster sites that were installed specifically for validation of the 3-km SMAP radar SM. The YE and YF focus areas provided mixed scenarios of cropping and grazing lands. In order to intercompare with Aquarius, a flight area of $95 \text{ km} \times 116 \text{ km}$ covering the ground sampling area was designed for a 3 dB footprint of Beam 2 of the Aquarius radiometer, having an incidence angle similar to SMAP.

The airborne and ground sampling was designed to be coincident with SMAP radar and radiometer coverage [32] such that the three orbits in each 8 days cycle over the study areas would be sampled when possible. Due to SMAP operational problems and weather conditions, a total of 15 flights were conducted over the SMAP validation flight area during the SMAPEX-4 and -5, with one dedicated flight over the Aquarius validation flight area during SMAPEX-4; 14 of the flights were coincident with SMAP coverage. The SM, vegetation, and surface roughness data were collected as planned, such that each of the six 3-km focus areas was revisited more than once per week during the SMAPEX-4 and -5, while the regional SM was repeated along the same route approximately twice per week. The schedule of airborne ground sampling activities in SMAPEX-4 and -5 is summarized together with overpasses of SMAP, SMOS, and Aquarius in Table II.

D. Airborne Sampling

During SMAPEX-4 and -5, the PLMR, PLIS, and supplementary sensors onboard the scientific aircraft were flown at an altitude of 3000 m above the ground, resulting in a nominal swath of 6 km. A spatial resolution of 1 km was achieved for PLMR and the multispectral sensors, while PLIS had a resolution of $\sim 10 \text{ m}$ over the $\sim 2 \text{ km}$ swath on either side of the flight track with a 2 km gap in the middle. Flight lines were

designed in a north–south direction with a spacing of 5 km, such that the outer 1 km of each swath was overlapped between adjacent flight lines, ensuring full coverage for PLMR over the entire SMAP validation flight area and full coverage of PLIS over all six focus areas (Fig. 1).

Being limited by the maximum flight duration, one of every three 5-km spaced flight lines over the Aquarius validation flight area was omitted, such that 72% and 47% of the Aquarius validation area was covered by PLMR and PLIS, respectively. According to a previous study [33], the averaged 1-km PLMR brightness temperature observations with more than half coverage are expected to still represent the space-borne brightness temperature observation with sufficient accuracy for validation of the low-resolution satellite observations.

Each flight was conducted over an approximately 6-h time window from 3 A.M. to 9 A.M. (local time), in order to minimize temporal deviation from the SMAP (and SMOS/Aquarius) nominal local overpass time of 6 A.M. To quantify the effect of this temporal deviation of brightness temperature observations, overflight of the Y3 site and a repeat pass for 20 km of the first north–south scan flight line were undertaken at the start and end of each flight.

During the SMAPEX-4 and -5, a total of 16 of the 17 scheduled flights were conducted, resulting in 14 concurrent pairs of SMAP and airborne observations; Flight 5 in SMAPEX-4 was canceled due to a rainfall event. Moreover, SMAP data corresponding to Flights 2 and 6 were lost in SMAPEX-4 due to problems with the star tracker and data downlink, respectively (Table II).

The calibrated airborne PLMR brightness temperature observations were corrected to the nominal 6 A.M. local overpass time of SMAP, SMOS, and Aquarius, using the soil temperature ratio of the actual time and the nominal 6 A.M. time. To compare with SMAP and Aquarius, the variable-angle PLIS backscatter and PLMR brightness temperature observations were normalized to the reference incidence angle of SMAP (40°) and the incidence angle of PLMR outer beams (38.5°), respectively, following [34]. Fig. 3 shows an example of the airborne 1-km brightness temperature (TB) observations and 10-m radar backscatter (σ_0) observations collected on May 10, 2015, together with the land use map; YA4 and YB5 represent the cropping and grazing scenarios. The PLMR brightness temperature shows the impact of land use types, which is also apparent in the PLIS backscatter.

Fig. 4 shows the examples of SMAPEX airborne and SMAP SM data collected at the start of SMAPEX-4 (May 2nd), at the end of SMAPEX-5 (September 26th), and on the day after each of the two rainfall events represented in the Australian Water Availability Project (AWAP) rainfall data during SMAPEX-4 [35]. The AWAP provides daily rainfall data accumulated from UTC time 23:00 P.M. on the day before to 23:00 P.M. on the current day, by grid interpolation to 0.25° from all available rain gauges. It is clear that SMAPEX-4 brightness temperature observations varied from a moderately dry homogeneous SM distribution (May 2, 2015) whose variation was dominated by topographic features [Column 1 in Fig. 4(a)], to heterogeneous SM conditions (May 19, 2015) that were mainly the result of the rainfall distribution pattern

TABLE II
SUMMARY OF THE SMAP/SMOS/AQUARIUS COVERAGE TOGETHER WITH THE SMAPEX AIRBORNE AND GROUND SAMPLING SCHEDULE

	COVERAGE				GROUND SAMPLING OF FOCUS AREAS			
	UTC Date	SMAP	SMOS	Aquarius Flight #	SM	Vegetation	Roughness	Vehicle-based
SMAPEX-4	May 02	AP	P	1	YA4, YB5, YF			YB5
	May 03	AP*	P	2	YA7, YB7, YE			YB7
	May 04				Regional	YA4, YA7	YA4	
	May 05	AP	P	3	YA4, YB5, YF			YB5
	May 06				Regional	YA4, YA7	YA7	
	May 07				Regional	YE, YF, YB	YB/YE/YF	
	May 10	AP	P	4	YA7, YB7, YE			YB7
	May 11	AP		5**	YA4, YB5, YF			YB5
	May 12				Regional	YA4, YA7	YA4	
	May 13	AP***	P	6	YA7, YB7, YE			YB7
	May 14				Regional	YA4, YA7	YA7	
	May 15		P		Regional	YE, YF, YB	YB/YE/YF	
	May 18	AP	P	7****	YA4, YB5, YF			YB5
	May 19	AP		8	YA7, YB7, YE			YB7
	May 20		P		Regional	YA4, YA7	YA	
May 21	AP	P	9	YA4, YB5, YF			YB5	
SMAPEX-5	Sep 08	P	P	1	YA4, YB5, YE			YB5
	Sep 09				Regional	YA4, YA7	YA4	
	Sep 10	P	P	2	YA7, YB7, YF			YB7
	Sep 11		P		Regional	YE, YF, YB	YA7	
	Sep 13	P	P	3	YA4, YB5, YE			YB5
	Sep 14				Regional	YA4, YA7	YB/YE/YF	
	Sep 15	P			Regional	YE, YF, YB	YA4	
	Sep 16	P	P	4	YA7, YB7, YF			YB7
	Sep 17				Regional	YA4, YA7	YB/YE/YF	
	Sep 18	P	P	5	YA4, YB5, YE			YB5
	Sep 21	P	P	6	YA7, YB7, YF			YB7
	Sep 22				Regional	YA4, YA7	YA4	
	Sep 23	P	P	7	YA4, YB5, YE			YB5
	Sep 24	P	P		Regional	YE, YF, YB	YB/YE/YF	
Sep 25				Regional	YA4, YA7	YA4		
Sep 26	P	P	8	YA7, YB7, YF			YB7	

A and P indicate radar (active) coverage and radiometer (passive) coverage respectively.

*: SMAP data were unavailable due to satellite downlink failure.

**: Flight was carried out over the Aquarius validation flight area.

***: SMAP data were unavailable due to problem with star tracks.

****: Flight was cancelled due to rainfall event.

[Column 3 in Fig. 4(a)]. Due to a heavy rainfall event on September 2, 2015 prior to the campaign start [Column 4 in Fig. 4(a)], SMAPEX-5 started from a very wet condition with localized flooding (September 8, 2015), followed by an ideal drying out period for monitoring changes in SM (e.g., September 26, 2015). A similar spatial pattern started between SMAPEX 1-km SM data [(Fig. 4(b))] and SMAP Level 2 SM products (Fig. 4(c)–(e)]. Consequently, the SMAPEX-4 and -5 data sets provide airborne brightness temperature and backscatter observations with a large spatial and temporal variability that are ideal for a comprehensive validation of SMAP and intercomparison with other space-borne radiometers, under a variety of SM, land surface types, and topography conditions.

E. Ground Sampling

The ground sampling data include spatial measurements of SM, vegetation, and surface roughness, which provide ground

truth and ancillary data for calibration and validation of SM retrieval from SMAPEX airborne observations.

Intensive SM sampling was conducted coincident with airborne overflights using the Hydraprobe Data Acquisition System (HDAS) [36], [37] to measure the top 5 cm SM at predefined sampling points with 250 m spacing across each 3-km focus area. At each point, three replicate SM measurements were taken within 1 m distance, in an effort to account for sampling uncertainty and spatial heterogeneity. Additional land surface information on vegetation type, vegetation height, dew presence, and irrigation type was manually recorded for each sampling point in the HDAS. At the end of each intensive sampling day, three gravimetric soil samples were collected together with HDAS measurements, representing low, medium, and high SM within each sampled 3-km focus area, for the purpose of probe calibration. The comparison showed that an overall root-mean-squared error (RMSE) of better than $0.04 \text{ m}^3/\text{m}^3$ was achieved for individual HDAS

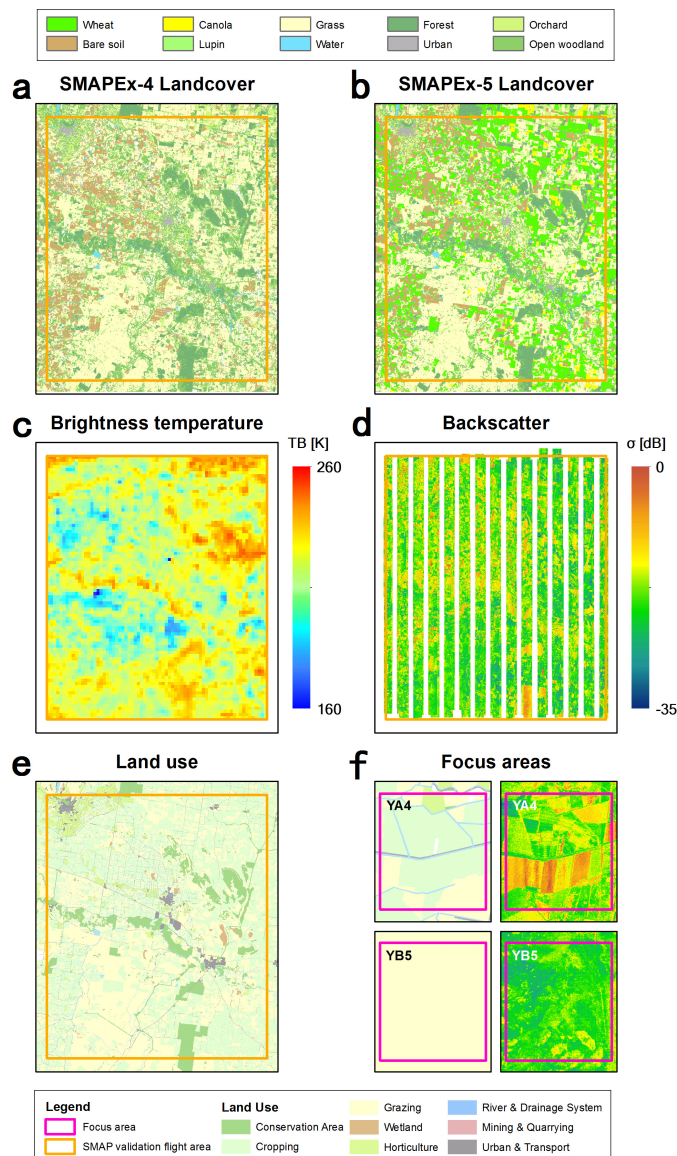


Fig. 3. Maps of land cover classification during (a) SMAPEX-4 and (b) SMAPEX-5, (c) airborne brightness temperature normalized to 38.5° , and (d) backscatter observations normalized to 40° over the SMAP validation flight area on May 11, 2015, as well as (e) land use. (Left) Zoomed-in view of land use. (Right) Backscatter observations over the YA4 and YB5 (f) focus areas.

measurements using a single calibration relationship [37], irrespective of the soil type. This is consistent with the results from earlier experiments.

To better understand the spatial variability of SM and to confirm the representativeness of the focus areas at the scale of the SMAP radiometer, regional ground SM sampling was conducted across the entire $36 \text{ km} \times 38 \text{ km}$ ground sampling area on the days without airborne sampling. A total of 40 representative sampling locations were selected along a $\sim 220 \text{ km}$ route with approximately 4 km spacing throughout the entire ground sampling area (Fig. 1), with three HDAS measurements made at each location.

Two types of vegetation sampling were conducted over the 3-km focus areas: spectral and intensive sampling. Spectral

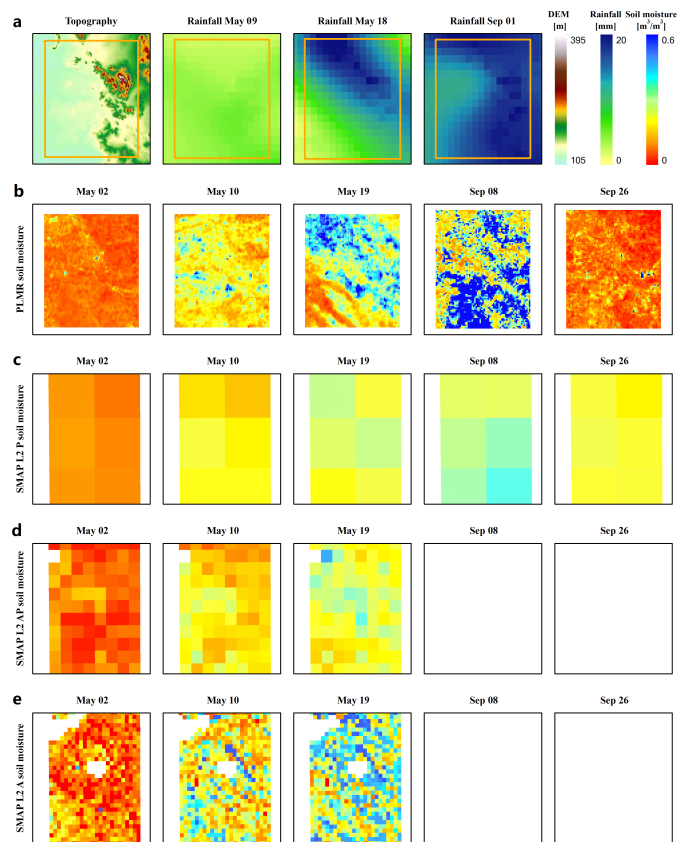


Fig. 4. (a) Topography (Column 1) and AWAP rainfall (Columns 2–4), (b) PLMR derived SM, (c) SMAP Level 2 Passive only derived SM, (d) Active/Passive derived SM, and (e) Active-only derived SM over the SMAP validation flight area during some example sampling days in SMAPEX-4 and -5. The white plots are due to failure of the SMAP radar on July 7, 2015.

vegetation sampling included spectral observations of plots together with destructive vegetation sampling, to confirm existing spectral relationships with VWC [38] of all dominant vegetation types at various stages of maturity. These measurements were made on a daily basis using a CropScan MSR16R. In addition, intensive vegetation sampling focused on detailed plant structural parameters of cropping and grazing areas for the purpose of radar algorithm development. The plant density and height, leaves and stalks dimension, orientation, and water content were sampled over dominant land surface types within the 3-km focus areas between the airborne sampling days. Given that the temporal variability of vegetation, vegetation biomass, VWC, surface reflectance, and structure were sampled with a revisit frequency of more than once per week, it was possible to accurately track the temporal variation of vegetation spectral and structural characteristics.

Soil surface roughness was measured at three locations within each major land surface type in the 3-km focus areas on the days without airborne sampling, using a pin profiler with 5-mm pin separation. At each sampling location, two 3-m-long surface height profiles were sampled in the north–south and west–east directions, respectively. Over furrowed areas, soil surface profiles were measured along and across the row direction, and recorded together with row orientation. For paddocks

that had farming activities during the experiment, soil surface roughness was periodically resampled.

In addition to conventional ground sampling, an innovative vehicle-based remote sensing platform was developed and used to measure soil and vegetation parameters with a very high resolution of approximately 2 m. It consisted of an L-band radiometer [the Eidgenössische Technische Hochschule (ETH) L-band radiometer for SM research ELBARA III] [39], [40], multispectral sensors (Skye visible/near infrared, short-wave infrared, and thermal infrared), the Light Airborne Reflectometer for GNSS-R Observations (LARGO) instrument [41], and electromagnetic induction (EMI) sensors including an EM38 ground conductivity meter [42] and Electromagnetic Conductivity Meter CMD-MiniExplorer [43]. To be comparable with SMAP, the ELBARA III was installed with a 40° incidence angle. Use of the vehicle-based remote sensing platform was limited to the YB area for logistical reasons, and driven in a north–south direction along the 250-m spacing SM sampling lines in YB5 and YB7, coincident with the intensive ground SM sampling.

As summarized in Table II, each of the six focus areas was visited at least four times for intensive SM and vegetation sampling during the 3 week period of each campaign, while regional SM sampling was repeated more than seven times during each campaign. Spectral vegetation and roughness sampling were carried out under typical vegetation types and land surface conditions across all six focus areas. Each focus area was visited several times in order to capture any changes after farming activities and irrigation.

Table III summarizes the statistics of SM, VWC, and surface roughness measurements for the dominant land surface types over the focus areas. A supervised land surface classification was applied to Landsat-8 imagery, using HDAS land cover information over the focus areas and the land surface of OzNet sites as ground truth (Fig. 3). The 30-m resolution land surface maps obtained for SMAPEX-4 and -5 were subsequently used in SM retrieval. During the austral autumn in SMAPEX-4, most crops had been harvested with dry/burned maize stubble and rice straw, with some farms plowed and ready to seed. This meant that the main land surface types were bare soil in the YA area and grass land in the YB area. High surface roughness values were measured under deep furrow conditions over harvested maize and in plowed paddocks. Moreover, winter wheat had been planted extensively in cropping areas and was at different growth stages ranging from seedling emergence during SMAPEX-4 to heading during SMAPEX-5.

SM and VWC were much higher in SMAPEX-5 than in SMAPEX-4, with high standard deviations of VWC due to high growth rates and heterogeneity. However, surface roughness was typically low during SMAPEX-5, since most of the furrowed cropping areas were harrowed flat for flood irrigation.

Fig. 5 shows an example of HDAS SM measurements in the YA4 and YB5 focus areas, demonstrating the spatial and temporal variation of SM in cropping and grazing areas, respectively. In addition, regional SM measurements collected on the day before or after the intensive sampling are also plotted. It is clear that the SM in the focus areas and the

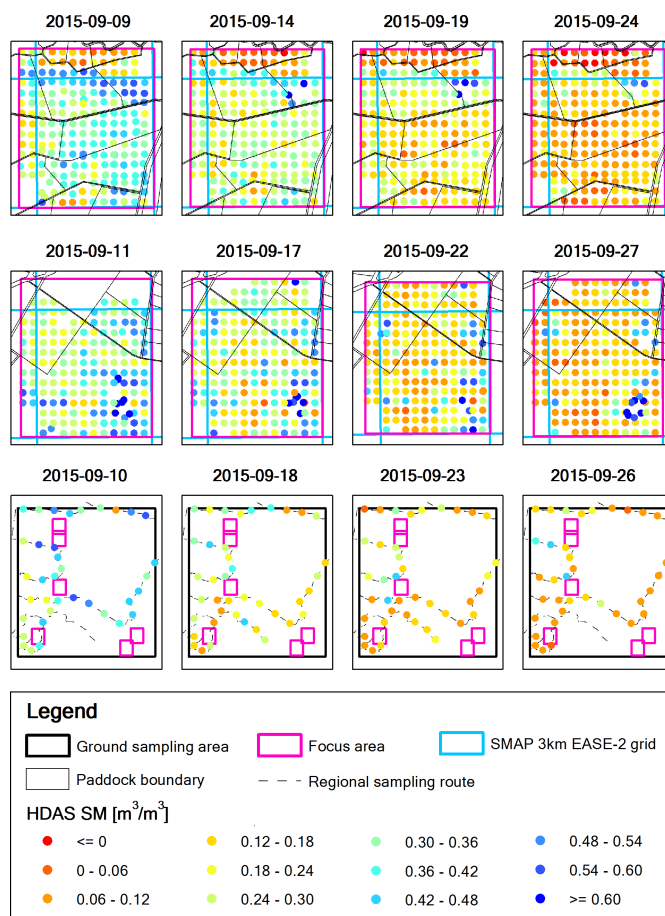


Fig. 5. Example of ground HDAS soil moisture measurements over YA4 (Row a), YB7 (Row b), and the regional sampling route (Row c) during the SMAPEX-5.

entire ground sampling area changed from wet and heterogeneous conditions to dry and relatively homogeneous conditions during SMAPEX-5, which matches with the observations at larger scale in Fig. 4. However, standing water (e.g., irrigated paddock in the northeast of YA4 and temporary pond in the southeast of YB7) was present and could induce SM retrieval error if not accurately accounted for [29].

F. Soil Moisture Retrieval

To validate and intercompare SMAP SM products, SM was retrieved from the dual polarized PLMR brightness temperature observations interpolated onto a 1 km grid at 40° incidence angle using the L-MEB model [44]. The 250-m MODIS daily reflectance products (MOD09GQ) were used to calculate the normalized difference vegetation index (NDVI) and, subsequently, estimate VWC over the study area using the relationships in Gao *et al.* [45]. Values for the few cloudy days were estimated by linear interpolation of the values from cloud-free data. The roughness and vegetation parameters used were obtained from previous studies in the Yanco area [46], [47], and literature for other land surface types within the study area [44], [48]. The 2.5- and 40-cm soil temperature measurements were averaged across the six temporary monitoring stations for use in estimating effective temperature.

TABLE III
SUMMARY STATISTICS OF THE GROUND MEASUREMENTS FOR THE MAIN TYPES OF LAND COVER

Land cover and fraction				Soil moisture [m ³ /m ³]		Vegetation water content [kg/m ²]		Surface RMS height [cm]		Roughness Correlation length [cm]	
Type	Cover fraction in SMAP validation flight area [%]	Cover fraction in focus area [%]	Mean	STD	Mean	STD	Mean	STD	Mean	STD	
SMAPEX-4	Bare soil	10.1	0.12	0.07	-	-	4.51	1.46	14.70	7.71	
	Wheat	0.0	0.0	-	-	1.18	0.80	-	-	-	
	Grass	45.5	58.0	0.13	0.06	0.29	0.21	3.12	1.8	18.92	6.39
	Canola	0.0	0.0	-	-	-	-	-	-	-	
	Lupin	0.0	0.0	-	-	0.02	0.01	-	-	-	
	Woodland	39.4	22.4	0.14	0.07	-	-	2.38	-	32.55	-
SMAPEX-5	Bare soil	9.6	0.21	0.11	-	-	2.92	1.81	12.08	4.77	
	Wheat	21.6	0.25	0.12	2.11	1.34	1.94	0.61	11.90	6.71	
	Grass	35.6	0.24	0.13	1.40	1.22	1.11	0.63	14.04	5.66	
	Canola	2.6	0.13	0.09	2.30	0.54	0.86	0.07	12.21	1.48	
	Lupin	0.1	0.06	0.06	2.32	0.11	0.64	0.02	17.55	13.65	
	Woodland	29.2	0.23	0.18	-	-	1.13	0.69	20.84	8.31	

STD stands for standard deviation.

The airborne SM retrieved from 1-km gridded PLMR brightness temperature was validated using the ground SM measurements over all six focus areas of SMAPEX-4 and -5. The intensive 250-m spacing HDAS SM measurements were averaged to the 1 km scale, and compared with retrieved SM at the pixel level for each land surface type as shown in Fig. 6. Due to the presence of standing water, overestimation of retrieved SM occurred (PLMR SM over 0.4 m³/m³) in some pixels. An overall RMSE of 0.08 m³/m³ was achieved for 1-km SMAPEX-4/-5 SM data using the published parameters.

III. EVALUATION OF SMAP PRODUCTS

A. Evaluation of SMAP L1 Products

The airborne radar and radiometer observations collected during SMAPEX-4 and -5 were compared with SMAP (and SMOS/Aquarius) radar and radiometer observations. The retrieved SM from airborne radiometer observations was used together with ground SM measurements to evaluate the SMAP EASE-2 SM products at the 3, 9, and 36 km scales.

The SMAPEX-4 and -5 airborne gridded brightness temperature observations, backscatter observations, and derived SM were averaged to the corresponding SMAP grid resolution, and compared with the SMAP L1C brightness temperature (R13080) and backscatter observations (R13080) products pixel by pixel. The comparison of brightness temperature in Fig. 7 shows a very good agreement between SMAP and PLMR with a correlation coefficient (R) close to 1. Taking PLMR averaged brightness temperature as the reference, an RMSE of ~ 2 K was achieved at the 36 km resolution for both polarizations in SMAPEX-4, increasing to ~ 5 K for horizontal polarization and ~ 3 K for vertical polarization in SMAPEX-5. According to the more detailed statistics summarized in Table IV, the bias of SMAP brightness temperature changed from -0.7 K in SMAPEX-4 and -4.5 K in SMAPEX-5, while the unbiased RMSE (ubRMSE) between PLMR and SMAP was stable at better than 3 K. In addition, airborne PLIS

backscatter observations were gridded and compared with SMAP L1C backscatter data at 1-km pixel level, achieving an overall RMSE of 3.41 dB during SMAPEX-4 with a bias of only around 0.5 dB.

B. Evaluation of SMAP L2 Products

SMAP SM products were validated using ground intensive SM measurements, the OzNet SM data, and the retrieved SM from airborne PLMR brightness temperature observations. Fig. 8 shows the comparison between the SMAP L2 Active SM products (R13080) at 3 km resolution and ground SM measurements over the six focus areas. The HDAS SM measurements at 250 m spacing were simply averaged to the S km EASE-2 grid and then compared with corresponding SMAP L2 active SM retrievals during the period of SMAPEX-4. The horizontal whiskers are the standard deviations of SM measurements within 3 km pixels, indicating the heterogeneity of the SM distribution and thus the uncertainty associated with the ground sampling. It is clear from Fig. 8 that the SMAP L2 Active SM product overestimated SM for all six focus areas and that the error was higher in wet than dry SM conditions.

Although the OzNet data have been used for long-term validation of SMAP Passive-only and Active-only SM products [23]–[26], it is still useful to provide this comparison as a reference, despite its shortcomings. Fig. 9 shows the time series of OzNet top 5-cm SM measurements from representative sites [49] together with SMAP L2 Passive-only (R13080), Active-only (R13080), and Active–Passive downscaled (D16000) SM products. The mean and 25th/75th percentiles of the SM measurements across the sites were calculated within the pixels of interest, to indicate spatial average and variability of SM within the given pixels. The SMAP L2 Passive SM product had a similar temporal evolution when compared with the SM measurements averaged from 28 OzNet sites. Overestimation occurred after rainfall events when VWC was relatively low. The same phenomenon was found between the SMAP L2 Active SM and OzNet top 5-cm

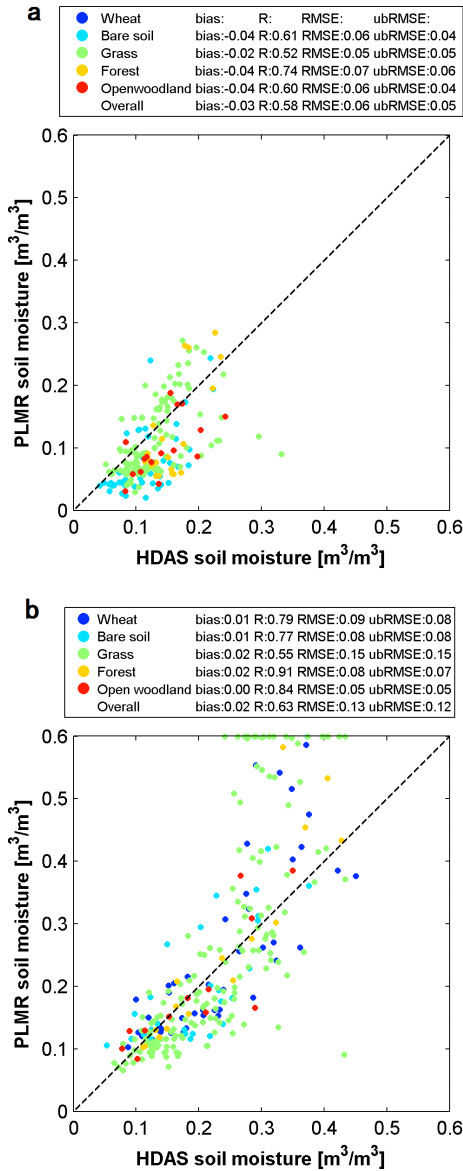


Fig. 6. Comparison between HDAS top 5-cm SM measurements and SM retrieved from the 1-km PLMR brightness temperature observations during (a) SMAPEX-4 and (b) SMAPEX-5 using published parameters.

SM measurements over cropping (YA) and grazing (YB) areas. A significant overestimation occurred after rainfall events on May 11, 2015 and May 20, 2015, which is consistent with the comparison result between the SMAP L2 Active SM and the ground HDAS SM measurements. Accordingly, the SMAP L2 Passive SM product was found to have an RMSE of 0.07 m^3/m^3 in SMAPEX-4 and 0.03 m^3/m^3 in SMAPEX-5, while the SMAP L2 Active SM product had an RMSE of 0.17 m^3/m^3 in SMAPEX-4. It can be seen from Table V that SMAP L2 SM products at all three scales had a poorer performance than PLMR SM data when compared with OzNet data, potentially due to the challenges of having representative point-based data, highlighting the importance of detailed spatial SM data such as that derived from PLMR.

Fig. 10 shows the scatter plots of PLMR SM as an independent reference against SMAP L2 SM products. The SMAP L2 Passive SM product shows a high correlation to the PLMR

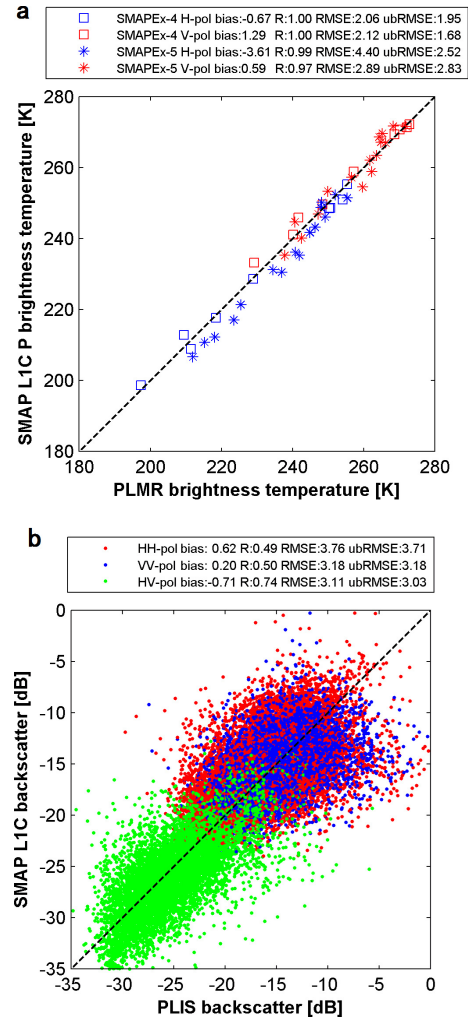


Fig. 7. Comparison of (a) SMAPEX-4 and -5 airborne PLMR brightness temperature and (b) PLIS backscatter observations with SMAP L1C radiometer and radar products, respectively.

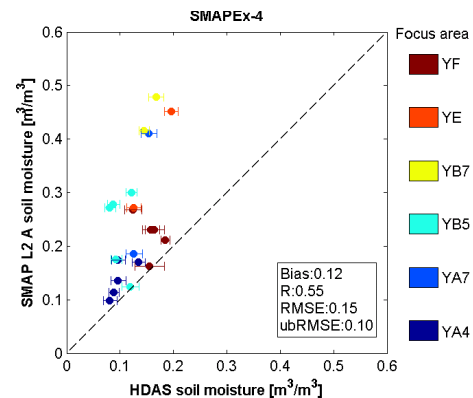


Fig. 8. Comparison between HDAS top 5-cm SM measurements and the 3-km SMAP L2 Active SM product over the six focus areas. The whiskers show the standard deviations of the ground measurements.

SM in both SMAPEX-4 and -5, with an R of better than 0.97 and an RMSE of better than 0.04 m^3/m^3 . However, the correlation coefficient R of SMAP L2 Active SM product against PLMR for SMAPEX-4 was much lower than for the

TABLE IV

STATISTICS OF THE RADAR BACKSCATTER (σ) AND RADIOMETER BRIGHTNESS TEMPERATURE (TB) DATA COMPARISON BETWEEN THE SPACE-BORNE PRODUCTS AND THE SMAPEX AIRBORNE AND GROUND OBSERVATIONS. BIAS, CORRELATION COEFFICIENT (R), RMSE, AND UBRMSE WERE CALCULATED FOR THE SMAPEX-4 (AND SMAPEX-5)

Bias [K]	SMAP L1B TB [K]	SMAP L1C TB [K]	SMOS L1C TB [K]	Aquarius L2 TB [K]	Bias [dB]	SMAP L1C σ [dB]
R [-]					R [-]	
RMSE [K]					RMSE [dB]	
ubRMSE [K]					ubRMSE [dB]	
PLMR TB in h-pol [K]	0.2 (-2.7)	-0.7 (-4.5)	6.4 (3.0)	5.4	PLIS σ in hh-pol [dB]	0.62 0.49 3.76 3.71
PLMR TB in v-pol [K]	2.3 (-0.4)	1.3 (-0.7)	-0.4 (-1.2)	4.8	PLIS σ in vv-pol [dB]	0.20 0.50 3.18 3.18
	0.99 (0.99)	1.00 (0.96)	0.99 (0.95)	-	PLIS σ in hv & vh-pol [dB]	-0.71 0.74 3.11 3.03
	2.6 (3.2)	2.0 (2.26)	7.5 (3.5)	-		
	2.6 (1.8)	2.0 (2.26)	3.9 (1.9)	-		
	3.0 (2.4)	2.2 (2.8)	1.9 (3.7)	-		
	1.9 (2.4)	1.8 (2.8)	1.9 (3.4)	-		

TABLE V

STATISTICS OF SM DATA COMPARISON BETWEEN THE SPACE-BORNE PRODUCTS AND THE SMAPEX AIRBORNE AND GROUND OBSERVATIONS. BIAS, CORRELATION COEFFICIENT (R), RMSE, AND UBRMSE WERE CALCULATED FOR THE SMAPEX-4 (AND SMAPEX-5)

Bias [m^3/m^3]	SMAP L2 P SM [m^3/m^3]	SMAP L2 AP SM [m^3/m^3]	SMAP L2 A SM [m^3/m^3]	SMOS L2 SM [m^3/m^3]	Aquarius L2 SM [m^3/m^3]
R [-]					
RMSE [m^3/m^3]					
ubRMSE [m^3/m^3]					
PLMR SM [m^3/m^3]	0.00 (0.02)	-0.02	0.03	0.02 (0.00)	-0.01
	0.95 (0.96)	0.77	0.6	0.98 (0.85)	-
	0.03 (0.06)	0.07	0.11	0.02 (0.06)	-
	0.03 (0.05)	0.07	0.11	0.02 (0.06)	-
	0.03 (0.02)	0.04	0.14	-	-
OzNet SM [m^3/m^3]	-0.18 (0.96)	0.73	0.56	-	-
	0.07 (0.03)	0.10	0.17	-	-
	0.06 (0.02)	0.10	0.10	-	-
	-	-	0.12	-	-
HDAS SM [m^3/m^3]	-	-	0.55	-	-
	-	-	0.15	-	-
	-	-	0.10	-	-

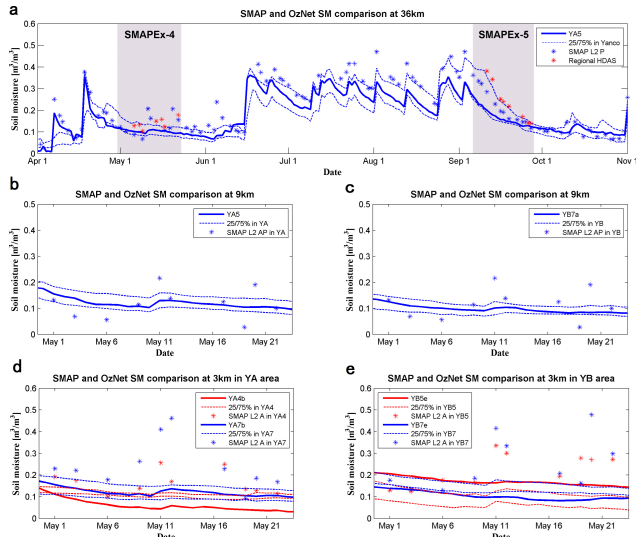


Fig. 9. Time series of top 5 cm SM from the OzNet sites, regional SM measurements during SMAPEX-4 and -5, and SMAP SM products at (a) 36 and (b) 9 km [(b) for YA cropping area and (c) for the YB grazing area] and (d) and (e) 3 km. The solid and dashed lines are SM measurements of the most representative sites [46] and 25th/75th percentiles of SM measurements across the OzNet sites, respectively, within the corresponding pixels.

passive product, with an RMSE of $0.11 \text{ m}^3/\text{m}^3$. As expected, the SMAP L2 Active/Passive SM product had an intermediate resolution with an intermediate accuracy.

IV. INTERCOMPARISON OF PLMR, SMAP, SMOS, AND AQUARIUS

The SMAP, SMOS, and Aquarius instruments use different radiometer techniques, providing L-band brightness temperature and SM products with different footprint geometries, revisit times, and accuracies. To examine their consistency and explore the possibility of integrating to a single long-term record, SMAP, SMOS, and Aquarius were intercompared against SMAPEX-4 and -5 airborne PLMR brightness temperature observations and retrieved SM.

A. Intercomparison of Brightness Temperature Observations

The incidence angle normalized airborne brightness temperature observations at 1 km resolution were averaged to the individual 3 dB footprints of the SMAP, SMOS, and Aquarius radiometers, and then compared with their brightness temperature products at the pixel level. The SMAP L1B (R16010), SMOS L1C (REPR), and Aquarius L2 (V4.0) brightness temperature products were compared with the PLMR brightness temperature observations during the SMAPEX-4 and -5. For SMOS, a second-degree polynomial relationship was used for each SMOS pixel to fit its angular relationship of L1C brightness temperature observations across the available range of incidence angles. Subsequently, the SMOS brightness temperature at the PLMR reference incidence angle of $\sim 40^\circ$ was

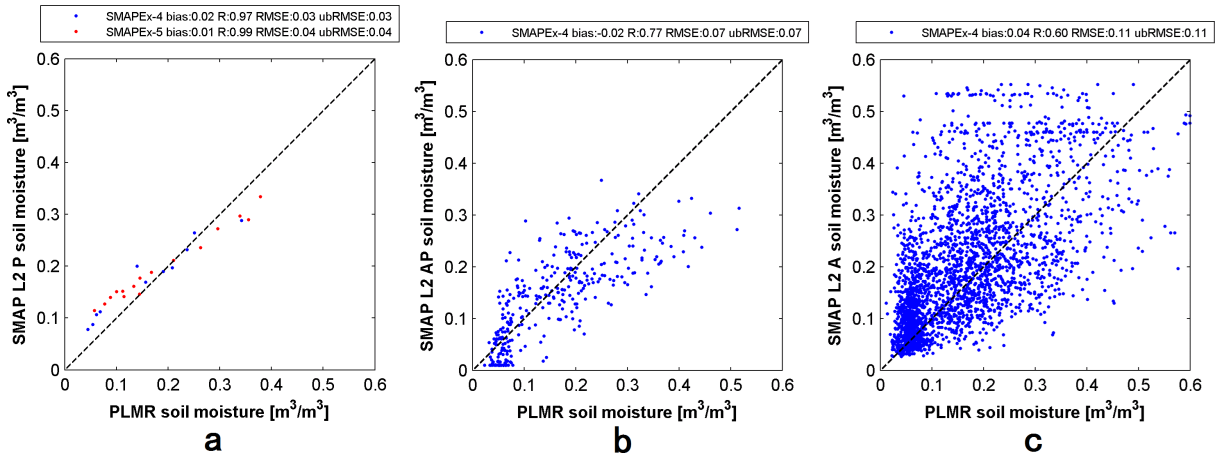


Fig. 10. Comparison of (a) SMAPEX-4 and -5 airborne PLMR SM versus SMAP L2 Passive/radiometer, (b) Active–Passive downscaled, and (c) Active/radar products.

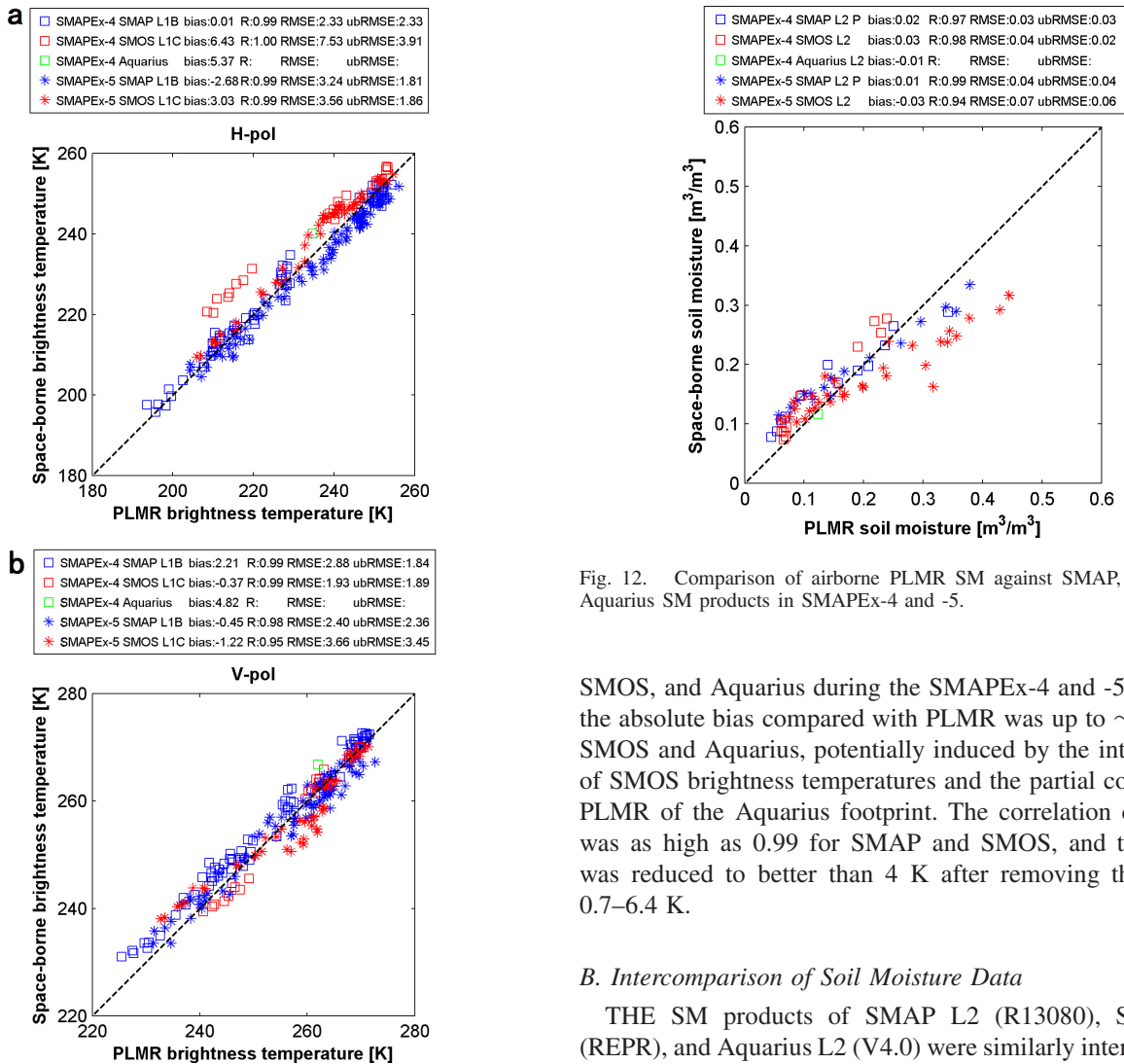


Fig. 11. Comparison of airborne PLMR brightness temperature observations against SMAP, SMOS, and Aquarius radiometer brightness temperature products for (a) horizontal and (b) vertical polarizations in SMAPEX-4 and -5.

interpolated from the polynomial function for the given pixel. The scatter plots in Fig. 11 and statistics in Table IV show a good agreement of brightness temperature among SMAP,

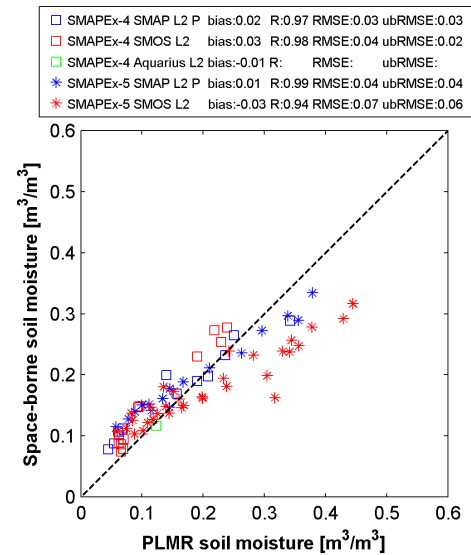


Fig. 12. Comparison of airborne PLMR SM against SMAP, SMOS, and Aquarius SM products in SMAPEX-4 and -5.

SMOS, and Aquarius during the SMAPEX-4 and -5, although the absolute bias compared with PLMR was up to ~6.5 K for SMOS and Aquarius, potentially induced by the interpolation of SMOS brightness temperatures and the partial coverage by PLMR of the Aquarius footprint. The correlation coefficient was as high as 0.99 for SMAP and SMOS, and the RMSE was reduced to better than 4 K after removing the bias of 0.7–6.4 K.

B. Intercomparison of Soil Moisture Data

THE SM products of SMAP L2 (R13080), SMOS L2 (REPR), and Aquarius L2 (V4.0) were similarly intercompared using the 1-km PLMR SM averaged to the respective footprints. Since SMAP does not provide SM retrieval for 3 dB footprints, the SMAP L2 Passive SM product on the 36-km EASE-2 grid was used in the intercomparison together with SMOS L2 and Aquarius L2 SM products on their elliptical footprints. Fig. 12 shows the intercomparison among SMAP, SMOS, and Aquarius SM products against PLMR SM for

TABLE VI

COMPARISON OF SMAP L2 PASSIVE AND ACTIVE SM PRODUCTS BETWEEN THE SMAP CORE VALIDATION SITES FROM [23] AND [24] AND SMAPEX DATA SETS. FOR SITES WITH MULTIPLE S KM PIXELS, ARITHMETIC AVERAGE OF STATISTICS IS SHOWN

	SMAP L2 passive (SCA-H)				SMAP L2 active			
	Bias [m ³ /m ³]	R [-]	RMSE [m ³ /m ³]	ubRMSE [m ³ /m ³]	Bias [m ³ /m ³]	R [-]	RMSE [m ³ /m ³]	ubRMSE [m ³ /m ³]
SMAPEX-4	0.00	0.95	0.03	0.03	0.03	0.60	0.11	0.11
SMAPEX-5	0.02	0.96	0.06	0.05	-	-	-	-
Yanco	0.02	0.94	0.06	0.06	-0.01	0.73	0.06	0.05
Kyeamba	0.04	0.93	0.07	0.05	-	-	-	-
Reynolds Creek	-0.07	0.48	0.08	0.05	-	-	-	-
Walnut Gulch	-0.02	0.58	0.04	0.03	0.01	-0.20	0.03	0.02
TxSON	-0.04	0.94	0.06	0.04	-0.03	0.76	0.06	0.05
Fort Cobb	-0.08	0.86	0.09	0.04	-	-	-	-
Little Washita	-0.06	0.93	0.06	0.03	-	-	-	-
South Fork	-0.08	0.56	0.10	0.06	-	-	-	-
Little River	0.03	0.84	0.04	0.03	-	-	-	-
Kenaston	-0.08	0.67	0.08	0.04	-0.03	0.34	0.10	0.10
Carman	-0.09	0.61	0.12	0.08	-	-	-	-
Monte Buey	-0.04	0.81	0.06	0.04	-0.02	0.59	0.08	0.08
REMEDHUS	-0.06	0.58	0.07	0.04	-	-	-	-

SMAPEX-4 and -5. The SM products of SMAP, SMOS, and Aquarius show correlation coefficients of better than 0.85 and RMSE between 0.03 and 0.07 m³/m³ during SMAPEX-4 and -5 (Table V).

V. DISCUSSION

Since the launch of SMAP, a number of SMAP postlaunch validation studies have been undertaken using station-based SM data [23]–[25]. SM data from different monitoring stations distributed within the same SMAP pixel were upscaled, and then used for temporal comparison with the SMAP products. Table VI shows the comparison of SMAP SM products against SM measurements from SMAP core sites and SMAPEX data set. A consistency of validation results between SMAPEX and Yanco core sites confirmed the representativeness of the Yanco sites at the scales of SMAP radiometer and radar. Due to their different land surface conditions and network configurations, other SMAP core sites showed diverse statistical results. As a complement to temporal validation of SMAP, the SMAPEX-4/-5 data provide L-band airborne radar backscatter and radiometer brightness temperature observations with higher spatial resolution and with full coverage over SMAP radar and radiometer footprints. Regular airborne radar and radiometer calibration and intensive ground SM sampling ensure the accuracy and consistency of the SMAPEX airborne observations and retrieved SM. Therefore, the SMAPEX-4 and -5 data sets were used as an independent reference for SMAP in-orbit validation under a range of land surface conditions.

According to scatter plots (Fig. 7) and statistics (Table IV) between SMAPEX and SMAP L1 radar backscatter and radiometer brightness temperature observations, the PLMR had a good agreement to SMAP radiometer in both polarizations with an R of better than 0.96, and an ubRMSE of better than 2.8 K during the SMAPEX-4 and -5. Due to: 1) its high resolution; 2) high sensitivity to surface roughness; 3) scattering of vegetation layer; and 4) uncertainty caused by incidence angle normalization, the SMAP radar had a lower

R of 0.82 and an ubRMSE of 3.41 dB in comparison with PLIS. There was no major variation of SMAP L1 data accuracies between SMAPEX-4 and -5. In short, the comparison between SMAP and PLIS was slightly poorer than the SMAP target accuracy of 0.7 dB for the radar and 1.3 K for the radiometer.

The SMAP L2 SM products were evaluated using ground intensive SM measurements (Fig. 8), OzNet monitoring station data (Fig. 9), and PLMR retrieved SM data (Fig. 10). Due to the presence of standing water in the YB grassland area at the beginning of SMAPEX-5, and flood irrigation in the YA wheat paddocks at the end of SMAPEX-5, the PLMR retrieved SMs were overestimated for wheat and grassland in these areas when SM was over 0.3 m³/m³ (Fig. 6). It is clear from Figs. 8–10 that the SMAP L2 Active SM product was overestimated with a bias of up to 0.14 m³/m³, having an R as low as 0.55 and an ubRMSE of \sim 0.1 m³/m³. In contrast, the SMAP L2 Passive SM product had an R of better than 0.95 and an ubRMSE of better than 0.06 m³/m³. As expected, the SMAP L2 Active/Passive SM product had an accuracy in between, with an R of better than 0.73 and an ubRMSE of better than 0.1 m³/m³. Taking the SMAP SM target accuracy of 0.04 m³/m³ as a benchmark, only the SMAP L2 Passive product met the requirement (in SMAPEX-4) when compared with PLMR retrieved SM. Compared with OzNet SM data in SMAPEX-5, the SMAP L2 Passive SM product showed a high accuracy.

In addition to SMAP in-orbit validation, the SMAPEX-4 data set provided a unique opportunity to intercompare among SMAP, SMOS, and Aquarius radiometer observations at their respective scales. Figs. 11 and 12 show the comparison of brightness temperature and retrieved SM between PLMR, SMAP, SMOS, and Aquarius. All space-borne radiometers had similar trends to PLMR with an R of better than 0.99. However, SMOS had a considerable and constant brightness temperature difference of \sim 5 K compared with SMAP in both SMAPEX-4 and -5, which may result from different radiometer concepts. In addition, SMOS SM accuracy compared with

TABLE VII

STATISTICS OF SM, BRIGHTNESS TEMPERATURE (TB), AND BACKSCATTER (σ) PRODUCTS FROM MULTIPLE SENSORS OVER THE YANCO SITE IN THE LAST 15 YEARS. ONLY MORNING OVERPASS RESULTS ARE SHOWN

Ref	Data set	Sensor	Product	Unit	Algorithm	Period	Bias	R	RMSE	ubRMSE
[50]	NAFE'06	AMSR-E	SM	[m ³ /m ³]	LPRM	Oct - Nov 2006	-	0.94	0.04	-
[51]	OzNet M8	AMSR-E	SM	[m ³ /m ³]	VUA-NASA	Jan - Dec 2006	0.07	0.88	0.09	0.02
[52]	AACES	SMOS	SM	[m ³ /m ³]	CATDS	Jan - Feb 2010, Sep 2010	0.05	-	-	-
[53]	OzNet Yanco	AMSR2	SM	[m ³ /m ³]	SCA	Jun 2012 - Jun 2016	0.02	0.61	0.06	0.05
[54]	OzNet Yanco	AMSR2	SM	[m ³ /m ³]	JAXA	Jul 2012 - Jul 2014	-0.05	0.49	0.07	0.05
		AMSR2			LPRM		0.07	0.65	0.10	0.07
		SMOS			CATDS		0.04	0.80	0.07	0.06
					Active/Passive		3.28	0.85	10.69	10.10
					Enhanced		3.29	0.92	7.42	6.49
[55]	SMAPEX	SMAP	Downscaled TB	[K]	Nearest neighbour	May 2015, Sep 2015	3.22	0.92	7.47	6.57
					Weighted average		1.04	0.92	7.02	6.74
					SFIM		3.16	0.93	7.22	6.18
					SMAP MOEA		-0.02	0.86	0.07	0.05
					SMAP A/P		-0.02	0.71	0.10	0.06
					SMOS DisPATchA		-0.04	0.16	0.13	0.11
					SMOS DisPATchD		-0.03	0.31	0.12	0.10
					SMAP VTCI		-0.07	0.09	0.16	0.14
					SMOS VTCI		-0.04	0.91	0.06	0.04
[56]	SMAPEX	SMAP	Downscaled SM	[m ³ /m ³]	SMAP SFIM	May 2015, Sep 2015	-0.03	0.40	0.11	0.10
					SMAP EnhancedA		-0.05	0.38	0.11	0.10
					SMAP EnhancedD		-0.04	0.46	0.11	0.09
					SMAP PassiveA		-0.07	0.19	0.14	0.12
					SMAP PassiveD		-0.05	0.43	0.12	0.10
					SMOS PassiveA		-0.05	0.26	0.13	0.11
					SMOS PassiveD		-0.05	0.38	0.12	0.10
			TB	[K]	L1C		-0.80	0.99	3.08	2.22
This paper	SMAPEX	SMAP	σ	[dB]	L1C	May 2015, Sep 2015	0.04	0.58	3.35	3.31
			SM	[m ³ /m ³]	L2 P		0.01	0.96	0.05	0.04
			SM	[m ³ /m ³]	L2 A		0.03	0.06	0.11	0.11
			SM	[m ³ /m ³]	L2 AP		-0.02	0.77	0.07	0.07

PLMR retrieval was considerably degraded in SMAPEX-5, potentially due to the impact of the standing water on SMOS. Importantly, the SMAP, SMOS, and Aquarius radiometer observations showed a high similarity, implying there is a potential to combine these three satellites observations for a long term and consistent SM time series data set.

The Yanco study area has been used to validate the performance of SM products derived from a number of space-borne missions over the last 15 years, including SMAP, SMOS, AMSR2, and AMSR-E. Table VII summarizes the satellite calibration and validation results from these studies and compares with those from this article. A series of validation studies over the Yanco area suggested: 1) a good agreement and a high consistency between the long-term monitoring station data and space-borne observations; 2) a considerable improvement in SM retrieval accuracy at L-band than higher frequencies; and 3) a higher correlation between space-borne products and airborne observations with a full coverage of satellites footprints than point-based monitoring station data. In this study, the performance of SMAP was only assessed over a range of typical cropping and grazing areas in Australia, using airborne observations collected during two limited periods in autumn and spring. In addition, only the early version of SMAP products was evaluated here. In order to test the full performance of SMAP, comparison between Single Channel Algorithms (SCA-H and SCA-V) and the Modified Dual Channel Algorithm (MDCA) is being conducted using the SMAPEX data sets, while evaluation with similar airborne

field experiments under different land surface conditions and in different seasons is being undertaken elsewhere.

VI. CONCLUSION

The SMAPEX-4 and -5 were conducted soon after completion of the SMAP commissioning phase, providing extensive data sets of airborne L-band microwave observations and concurrent ground measurements of SM, for the purpose of SMAP postlaunch validation and intercomparison with SMOS and Aquarius. As a complement to temporal validation studies of SMAP using the OzNet stations, the SMAPEX-4/-5 data set was used to validate the SMAP radar and radiometer SM products over the study area in the Murrumbidgee River Catchment. Due to the SMAP radar failure on July 7, 2015, the SMAPEX-4 was the only extensive field campaign worldwide to provide such a unique opportunity for validation of the SMAP L2 Active-only SM product and the SMAP L2 Active-Passive downscaled SM product. The high-resolution SMAPEX airborne radar, radiometer, and retrieved SM data were aggregated and used as an independent reference to evaluate the SMAP L1 and L2 products at their respective scales. The results showed a good in-orbit performance of SMAP under Australian land surface conditions during the two 3-week-long experiments in the austral autumn and spring. An R of better than 0.98, and an ubRMSE of better than 3 K were achieved for the SMAP radiometer brightness temperature observations, and an R of 0.82 and RMSE of 3.4 dB were achieved for the SMAP radar backscatter observations.

Given the uncertainty caused by temporal variation of the land surface during the flights, incidence angle normalization, and antenna pattern, SMAP achieved a level of accuracy similar to its target accuracies of 1.3 K for the radiometer and 0.5 dB for the radar. The $0.04 \text{ m}^3/\text{m}^3$ target accuracy for SM was satisfied for the SMAP Passive SM product during SMAPEX-4 ($0.03 \text{ m}^3/\text{m}^3$), while slightly lowered during SMAPEX-5 ($0.06 \text{ m}^3/\text{m}^3$) due to the presence of standing water. As expected, the accuracy of SMAP Active and Active–Passive downscaled SM products was lower with R values of 0.6 and 0.77, and with ubRMSEs of 0.11 and $0.07 \text{ m}^3/\text{m}^3$, respectively. Due to its reduced representativeness, the OzNet SM data showed a lower SMAP performance than the SMAPEX airborne SM data during the SMAPEX-4/-5 periods but with similar statistics to the long-term validation results of the Yanco core site [25].

In addition, the SMAP, SMOS, and Aquarius radiometer brightness temperature and SM products were intercompared against the SMAPEX airborne brightness temperature observations and SM data aggregated to their 3 dB footprints. Although only one flight was conducted over an Aquarius 3 dB footprint, with 72% coverage, the intercomparison results showed a good agreement among SMAP, SMOS, and Aquarius in terms of brightness temperature with R values of better than 0.9 and RMSE values of better than ~ 7.5 K. In terms of SM, the R values were better than 0.85 and RMSE values were better than $0.07 \text{ m}^3/\text{m}^3$. Consequently, this analysis has showed a considerable consistency among SMAP, SMOS, and Aquarius, and confirmed the potential of generating a long-term SM record by combining them. However, further studies and airborne field experiments are required for SMAP validation and intercomparison under other land surface conditions. The SMAPEX-4/-5 data sets presented and used in this article are publicly available at <http://www.smapex.monash.edu.au>.

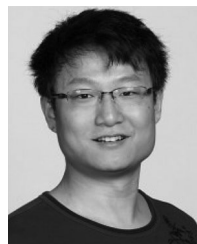
ACKNOWLEDGMENT

The authors would like to thank all the SMAPEX-4 and -5 experiment participants: C. Abolt, C. Amat, C. Callipari, J. Cardona, W. Chaivanont, A. Colliander, P. Daniel, S. Dey, R. Esmaili, A. Fattore, J. Fayne, A. Gevaert, S. Grimaldi, M. Hassan, A. Heidari, C. Holifield, J. Johanson, A. Joseph, A. Kentaro, S. Kim, T. Larson, M. Lewis, F. Li, Y. Li, Y. Liu, Y. Malbêteau, I. Marang, A. Marks, L. McKee, A. McNally, G. Nearing, K. Newtoff, R. Onrubia, R. Parinussa, J. Park, E. Podest, P. Pohlig, J. Prueger, A. Purdy, M. de Quadras, D. Smith, V. Stefan, S. Tian, A. White, F. Winston, A. Wright, and Z. Yazdanfar. The ELBARA III and the LARGO instruments were provided by the Terrestrial Environmental Observatories (TERENO) and the Advanced Remote Sensing—Ground-Truth Demo and Test Facilities (ACROSS) funded by the Helmholtz Association of German Research Centres (HGF).

REFERENCES

- [1] D. Aubert, C. Loumagne, and L. Oudin, "Sequential assimilation of soil moisture and streamflow data in a conceptual rainfall–runoff model," *J. Hydrol.*, vol. 280, nos. 1–4, pp. 145–161, 2003.
- [2] A. Olioso, H. Chauki, D. Courault, and J.-P. Wigneron, "Estimation of evapotranspiration and photosynthesis by assimilation of remote sensing data into SVAT models," *Remote Sens. Environ.*, vol. 68, no. 3, pp. 341–356, Jun. 1999.
- [3] J. Schnürer, M. Clarholm, S. Boström, and T. Rosswall, "Effects of moisture on soil microorganisms and nematodes: A field experiment," *Microbial Ecol.*, vol. 12, no. 2, pp. 217–230, Jun. 1986.
- [4] P. J. Sellers, "Modeling the exchanges of energy, water, and carbon between continents and the atmosphere," *Science*, vol. 275, no. 5299, pp. 502–509, Jan. 1997.
- [5] W. T. Crow *et al.*, "Upscaling sparse ground-based soil moisture observations for the validation of coarse-resolution satellite soil moisture products," *Rev. Geophys.*, vol. 50, no. 2, Jun. 2012.
- [6] D. Ryu and J. S. Famiglietti, "Multi-scale spatial correlation and scaling behavior of surface soil moisture," *Geophys. Res. Lett.*, vol. 33, no. 8, 2006.
- [7] T. J. Jackson and T. J. Schmugge, "Passive microwave remote sensing system for soil moisture: Some supporting research," *IEEE Trans. Geosci. Remote Sens.*, vol. 27, no. 2, pp. 225–235, Mar. 1989.
- [8] E. G. Njoku *et al.*, "Observations of soil moisture using a passive and active low-frequency microwave airborne sensor during SGP99," *IEEE Trans. Geosci. Remote Sens.*, vol. 40, no. 12, pp. 2659–2673, Dec. 2002.
- [9] Y. H. Kerr *et al.*, "The SMOS mission: New tool for monitoring key elements of the global water cycle," *Proc. IEEE*, vol. 98, no. 5, pp. 666–687, May 2010.
- [10] D. Entekhabi *et al.*, "The soil moisture active passive (SMAP) mission," *Proc. IEEE*, vol. 98, no. 5, pp. 704–716, May 2010.
- [11] J. Shi *et al.*, "WCOM: The science scenario and objectives of a global water cycle observation mission," in *Proc. IEEE Geosci. Remote Sens. Symp.*, Jul. 2014, pp. 3646–3649.
- [12] T. Zhao *et al.*, "Soil moisture experiment in the Luan River supporting new satellite mission opportunities," *Remote Sens. Environ.*, vol. 240, Apr. 2020, Art. no. 111680.
- [13] J. Jacobs, "SMEX02: Field scale variability, time stability and similarity of soil moisture," *Remote Sens. Environ.*, vol. 92, no. 4, pp. 436–446, Sep. 2004.
- [14] T. J. Jackson *et al.*, "Polarimetric scanning radiometer C-and X-band microwave observations during SMEX03," *IEEE Trans. Geosci. Remote Sens.*, vol. 43, no. 11, pp. 2418–2430, Nov. 2005.
- [15] R. Bindlish, T. Jackson, R. Sun, M. Cosh, S. Yueh, and S. Dinardo, "Combined passive and active microwave observations of soil moisture during CLASIC," *IEEE Geosci. Remote Sens. Lett.*, vol. 6, no. 4, pp. 644–648, Oct. 2009.
- [16] H. McNairn *et al.*, "The soil moisture active passive validation experiment 2012 (SMAPVEX12): Prelaunch calibration and validation of the SMAP soil moisture algorithms," *IEEE Trans. Geosci. Remote Sens.*, vol. 53, no. 5, pp. 2784–2801, May 2015.
- [17] R. Panciera *et al.*, "The soil moisture active passive experiments (SMAPEX): Toward soil moisture retrieval from the SMAP mission," *IEEE Trans. Geosci. Remote Sens.*, vol. 52, no. 1, pp. 490–507, Jan. 2014.
- [18] G. Lagerloef, F. Wentz, S. Yueh, H. Kao, G. Johnson, and J. Lyman, "Aquarius satellite mission provides new, detailed view of sea surface salinity," *Bull. Amer. Meteorol. Soc.*, vol. 93, no. 7, pp. S70–S71, 2012.
- [19] R. Bindlish, T. Jackson, M. Cosh, T. Zhao, and P. O'Neill, "Global soil moisture from the Aquarius/SAC-D satellite: Description and initial assessment," *IEEE Geosci. Remote Sens. Lett.*, vol. 12, no. 5, pp. 923–927, May 2015.
- [20] Y. Y. Liu *et al.*, "Developing an improved soil moisture dataset by blending passive and active microwave satellite-based retrievals," *Hydrol. Earth Syst. Sci.*, vol. 15, no. 2, pp. 425–436, Feb. 2011.
- [21] L. Zhu *et al.*, "The polarimetric L-band imaging synthetic aperture radar (PLIS): Description, calibration, and cross-validation," *IEEE J. Sel. Topics Appl. Earth Observ. Remote Sens.*, vol. 11, no. 11, pp. 4513–4525, Nov. 2018.
- [22] A. B. Smith *et al.*, "The murrumbidgee soil moisture monitoring network data set," *Water Resour. Res.*, vol. 48, no. 7, Jul. 2012, Art. no. W07701.
- [23] S. K. Chan *et al.*, "Assessment of the SMAP passive soil moisture product," *IEEE Trans. Geosci. Remote Sens.*, vol. 54, no. 8, pp. 4994–5007, Aug. 2016.
- [24] S. Kim *et al.*, "Surface soil moisture retrieval using the L-band synthetic aperture radar onboard the soil moisture active–passive satellite and evaluation at core validation sites," *IEEE Trans. Geosci. Remote Sens.*, vol. 55, no. 4, pp. 1897–1914, Apr. 2017.

- [25] A. Colliander *et al.*, "Validation of SMAP surface soil moisture products with core validation sites," *Remote Sens. Environ.*, vol. 191, pp. 215–231, Mar. 2017.
- [26] A. Colliander *et al.*, "An assessment of the differences between spatial resolution and grid size for the SMAP enhanced soil moisture product over homogeneous sites," *Remote Sens. Environ.*, vol. 207, pp. 65–70, Mar. 2018.
- [27] O. Merlin *et al.*, "The NAFE'06 data set: Towards soil moisture retrieval at intermediate resolution," *Adv. Water Resour.*, vol. 31, no. 11, pp. 1444–1455, 2008.
- [28] S. Peischl *et al.*, "The ACES field experiments: SMOS calibration and validation across the murrumbidgee river catchment," *Hydrol. Earth Syst. Sci. Discuss.*, vol. 9, no. 3, pp. 2763–2795, Mar. 2012.
- [29] N. Ye, J. P. Walker, J. Guerschman, D. Ryu, and R. J. Gurney, "Standing water effect on soil moisture retrieval from L-band passive microwave observations," *Remote Sens. Environ.*, vol. 169, pp. 232–242, Nov. 2015.
- [30] N. Ye, J. P. Walker, C. Rüdiger, D. Ryu, and R. J. Gurney, "Surface rock effects on soil moisture retrieval from L-band passive microwave observations," *Remote Sens. Environ.*, vol. 215, pp. 33–43, Sep. 2018.
- [31] N. Ye, J. P. Walker, C. Rudiger, D. Ryu, and R. J. Gurney, "Impact of urban cover fraction on SMOS and SMAP surface soil moisture retrieval accuracy," *IEEE J. Sel. Topics Appl. Earth Observ. Remote Sens.*, vol. 12, no. 9, pp. 3338–3350, Sep. 2019.
- [32] M. Spencer, S. Chan, L. Veilleux, and K. Wheeler, "The soil moisture Active/Passive (SMAP) mission radar: A novel conically scanning SAR," in *Proc. IEEE Radar Conf.*, May 2009, pp. 1–4.
- [33] C. Rudiger, J. P. Walker, and Y. H. Kerr, "On the airborne spatial coverage requirement for microwave satellite validation," *IEEE Geosci. Remote Sens. Lett.*, vol. 8, no. 4, pp. 824–828, Jul. 2011.
- [34] N. Ye, J. P. Walker, and C. Rudiger, "A cumulative distribution function method for normalizing variable-angle microwave observations," *IEEE Trans. Geosci. Remote Sens.*, vol. 53, no. 7, pp. 3906–3916, Jul. 2015.
- [35] D. A. Jones, W. Wang, and R. Fawcett, "High-quality spatial climate data-sets for Australia," *Austral. Meteorol. Oceanographic J.*, vol. 58, no. 4, p. 233, 2009.
- [36] R. Panciera, O. Merlin, R. Young, and J. Walker, "The hydraprobe data acquisition system (HDAS): User guide," Univ. Melbourne, Melbourne, VIC, Australia, Tech. Rep., 2006.
- [37] O. Merlin, J. P. Walker, R. Panciera, R. Young, J. D. Kalma, and E. J. Kim, "Calibration of a soil moisture sensor in heterogeneous terrain with the national airborne field experiment (NAFE) data," presented at the MODSIM Int. Congr. Modeling Simulation, Dec. 2007.
- [38] Y. Gao *et al.*, "Evaluation of the tau-omega model for passive microwave soil moisture retrieval using SMAPEX datasets," *IEEE J. Sel. Topics Appl. Earth Observ. Remote Sens.*, vol. 11, no. 3, pp. 888–895, Mar. 2018.
- [39] M. Schwank *et al.*, "ELBARA II, an L-band radiometer system for soil moisture research," *Sensors*, vol. 10, no. 1, pp. 584–612, Jan. 2010.
- [40] F. Jonard, L. Weiermuller, K. Z. Jadoon, M. Schwank, H. Vereecken, and S. Lambot, "Mapping field-scale soil moisture with L-band radiometer and ground-penetrating radar over bare soil," *IEEE Trans. Geosci. Remote Sens.*, vol. 49, no. 8, pp. 2863–2875, Aug. 2011.
- [41] A. Alonso-Arroyo *et al.*, "The light airborne reflectometer for GNSS-R observations (LARGO) instrument: Initial results from airborne and rover field campaigns," in *Proc. IEEE Geosci. Remote Sens. Symp.*, Jul. 2014, pp. 4054–4057.
- [42] *EM38-Ground Conductivity Meter-Operating Manual*, Geonics Limited, Mississauga, ON, Canada, 1999.
- [43] *CMD Electromagnetic Conductivity Meter User Manual V. 1.5. GF Instruments S.R.O. Geophysical Equipment and Services*, GF Instrum., s.r.o., Brno, Czech Republic, 2011.
- [44] J.-P. Wigneron *et al.*, "L-band microwave emission of the biosphere (L-MEB) model: Description and calibration against experimental data sets over crop fields," *Remote Sens. Environ.*, vol. 107, no. 4, pp. 639–655, Apr. 2007.
- [45] Y. Gao, J. P. Walker, M. Allahmoradi, A. Monerris, D. Ryu, and T. J. Jackson, "Optical sensing of vegetation water content: A synthesis study," *IEEE J. Sel. Topics Appl. Earth Observ. Remote Sens.*, vol. 8, no. 4, pp. 1456–1464, Apr. 2015.
- [46] R. Panciera *et al.*, "The NAFE'05/CoSMOS data set: Toward SMOS soil moisture retrieval, downscaling, and assimilation," *IEEE Trans. Geosci. Remote Sens.*, vol. 46, no. 3, pp. 736–745, Mar. 2008.
- [47] R. Panciera, J. P. Walker, J. D. Kalma, E. J. Kim, K. Saleh, and J.-P. Wigneron, "Evaluation of the SMOS L-MEB passive microwave soil moisture retrieval algorithm," *Remote Sens. Environ.*, vol. 113, no. 2, pp. 435–444, Feb. 2009.
- [48] J. P. Grant *et al.*, "Calibration of the L-MEB model over a coniferous and a deciduous forest," *IEEE Trans. Geosci. Remote Sens.*, vol. 46, no. 3, pp. 808–818, Mar. 2008.
- [49] M. S. Yee, J. P. Walker, A. Monerris, C. Rüdiger, and T. J. Jackson, "On the identification of representative *in situ* soil moisture monitoring stations for the validation of SMAP soil moisture products in Australia," *J. Hydrol.*, vol. 537, pp. 367–381, Jun. 2016.
- [50] I. Mladenova, V. Lakshmi, T. J. Jackson, J. P. Walker, O. Merlin, and R. A. M. de Jeu, "Validation of AMSR-E soil moisture using L-band airborne radiometer data from national airborne field experiment 2006," *Remote Sens. Environ.*, vol. 115, no. 8, pp. 2096–2103, Aug. 2011.
- [51] C. S. Draper, J. P. Walker, P. J. Steinle, R. A. De Jeu, and T. R. Holmes, "An evaluation of AMSR-E derived soil moisture over Australia," *Remote Sens. Environ.*, vol. 113, no. 4, pp. 703–710, 2009.
- [52] C. Rüdiger, J. Walker, Y. Kerr, A. Mialon, O. Merlin, and E. Kim, "Validation of the level 1c and level 2 SMOS products with airborne and ground-based observations," in *Proc. Int. Congr. Modeling Simulation (MODSIM)*, Perth, NSW, Australia, Dec. 2011, pp. 12–16.
- [53] R. Bindlish *et al.*, "GCOM-W AMSR2 soil moisture product validation using core validation sites," *IEEE J. Sel. Topics Appl. Earth Observ. Remote Sens.*, vol. 11, no. 1, pp. 209–219, Jan. 2018.
- [54] M. S. Yee, J. P. Walker, C. Rüdiger, R. M. Parinussa, T. Koike, and Y. H. Kerr, "A comparison of SMOS and AMSR2 soil moisture using representative sites of the OzNet monitoring network," *Remote Sens. Environ.*, vol. 195, pp. 297–312, Jun. 2017.
- [55] N. Ye *et al.*, "Evaluation of SMAP downscaled brightness temperature using SMAPEX-4/5 airborne observations," *Remote Sens. Environ.*, vol. 221, pp. 363–372, Feb. 2019.
- [56] S. Sabaghy *et al.*, "Comprehensive analysis of alternative downscaled soil moisture products," *Remote Sens. Environ.*, vol. 239, Mar. 2020, Art. no. 111586.



Nan Ye received the B.E. degree in hydraulic and hydropower engineering from Tsinghua University, Beijing, China, in 2006, and the Ph.D. degree in civil engineering from Monash University, Clayton, VIC, Australia, in 2014.

Then, he coordinated a number of airborne field experiments for the in-orbit calibration/validation of the Soil Moisture Active Passive mission in the Murrumbidgee River catchment, southeast of Australia. He is a Senior Research Fellow with Monash University, working on P-band passive microwave

remote sensing of soil moisture.



Jeffrey P. Walker (Fellow, IEEE) received the B.E. degree in civil engineering and the Bachelor of Surveying degree (Hons.) from The University of Newcastle, Callaghan, NSW, Australia, in 1995, and the Ph.D. degree in water resources engineering from the University of Newcastle in 1999.

He was with the National Aeronautics and Space Administration (NASA) Goddard Space Flight Centre, Greenbelt, MD, USA, to implement his soil moisture (SM) work globally. In 2001, he joined the Department of Civil and Environmental Engineering, University of Melbourne, Melbourne, VIC, Australia, as a Lecturer. Since 2010, he has been a Professor with the Department of Civil Engineering, Monash University, Clayton, VIC, where he is continuing his research. He is contributing to SM satellite missions at NASA, European Space Agency (ESA), and JAXA, as a Science Team Member for the Soil Moisture Active Passive mission and a Cal/Val Team Member for the Soil Moisture and Ocean Salinity and Global Change Observation Mission—Water, respectively.

Dr. Walker received the University Medal for Bachelor of Surveying from The University of Newcastle.



Xiaoling Wu (Member, IEEE) received the B.E. degree in biomedical engineering from Zhejiang University, Hangzhou, China, in 2009, and the Ph.D. degree in civil engineering from Monash University, Clayton, VIC, Australia, in 2015.

The topic of her undergraduate thesis was development of biosensor using nanomaterial. She was a Visiting Scholar with the Department of Computer Science, University of Copenhagen, Copenhagen, Denmark, from 2009 to 2010. The topic of her Ph.D. research was downscaling of soil moisture (SM) using airborne radar and radiometer observations in order to provide an accurate and high resolution (better than 10 km) SM product with potential benefit in the areas of weather forecasting, flood, drought prediction, and agricultural activities. She is the Research Fellow with Monash University and continuing high-resolution SM work. Her research interests include microwave remote sensing of SM, SM downscaling, and proximal SM sensing for real-time agricultural applications.



Richard de Jeu received the M.S. degree in environmental hydrology and the Ph.D. degree from VU University Amsterdam, Amsterdam, The Netherlands, in 1996 and 2003, respectively.

From 1997 to 1999, he was a Research Assistant with VU University Amsterdam. From 1999 to 2001, he was a Research Assistant with Goddard Space Flight Center, National Aeronautics and Space Administration, Greenbelt, MD, USA. Over the years, he successfully developed several satellite-derived data products including soil moisture and evaporation. These products are widely used and accessible through the official European Space Agency (ESA) and National Aeronautics and Space Administration (NASA) data portals. He has been involved in many projects supported by the Dutch Organization for Scientific Research, European Framework, and the European and American Space Agencies. He is a Managing Director with Transmissivity B.V./VanderSat B.V., Noordwijk, The Netherlands. His research interests include passive microwave radiometry and the use of this technique for hydrological applications.



Ying Gao (Member, IEEE) received the B.E. degree (Hons.) in civil engineering from Monash University, Clayton, VIC, Australia, and Central South University, Changsha, China, in 2010, and the Ph.D. degree in civil engineering from Monash University in 2016.

Since 2016, she has been a Research Fellow with Monash University. Her research interests include active and passive microwave remote sensing, optical sensing of vegetation, and surface roughness parameterization.



Thomas J. Jackson (Fellow, IEEE) received the Ph.D. degree from the University of Maryland, College Park, MD, USA, in 1976.

He is a Research Hydrologist with the U.S. Department of Agriculture, Agricultural Research Service, Hydrology and Remote Sensing Laboratory, Beltsville, MD, USA. He is a member of the science and validation teams of the Aqua, ADEOS-II, Radarsat, Oceansat-1, ENVISAT, ALOS, SMOS, Aquarius, GCOM-W, and SMAP remote sensing satellites. His research interests include the application and development of remote sensing technology in hydrology and agriculture, and primarily microwave measurement of soil moisture.

Dr. Jackson is a fellow of the Society of Photo-Optical Instrumentation Engineers, the American Meteorological Society, and the American Geophysical Union. He was a recipient of the William T. Pecora Award [National Aeronautics and Space Administration (NASA) and Department of Interior] in 2003 for outstanding contributions toward understanding the Earth by means of remote sensing, the AGU Hydrologic Sciences Award for outstanding contributions to the science of hydrology, and the IEEE Geoscience and Remote Sensing Society Distinguished Achievement Award in 2011.



François Jonard (Member, IEEE) received the M.Sc. and Ph.D. degrees in bioscience engineering from the University of Louvain (UCLouvain), Louvain-la-Neuve, Belgium, in 2002 and 2012, respectively.

In 2011, he joined NASA Goddard Space Flight Center, Greenbelt, MD, USA, as a Visiting Scientist, contributing to the preparation of the Soil Moisture Active and Passive (SMAP) mission. From 2018 to 2020, he was a Regular Visiting Scientist with the Massachusetts Institute of Technology (MIT), Cambridge, MA, USA. Since 2009, he has been with the Institute of Bio- and Geosciences (Agrosphere), Research Centre Jülich, Jülich, Germany. He is an Associate Professor with the Faculty of Bioscience Engineering, UCLouvain, and also a Lecturer with the Faculty of Sciences, University of Liège, Liège, Belgium. His research interests include terrestrial remote sensing (microwave and hyperspectral), ecohydrology, and hydrogeophysics.

Dr. Jonard was awarded the MIT-MISTI Grant for a project on the early detection of plant water stress using remote sensing.



Edward Kim (Senior Member, IEEE) received the S.B. and S.M. degrees in electrical engineering from the Massachusetts Institute of Technology, Cambridge, MA, USA, and a joint Ph.D. degree from the Department of Electrical Engineering and Atmospheric Sciences, University of Michigan, Ann Arbor, MI, USA, in 1998.

Since 1999, he has been with National Aeronautics and Space Administration (NASA) Goddard Space Flight Center, Greenbelt, MD, USA, where he has been involved in remote sensing of snow, soil moisture, frozen soil, and the atmosphere as well as satellite mission development. His research interests include instrument development, field campaigns, electromagnetic modeling, retrieval algorithms, and calibration.

Dr. Kim served as the Project Scientist for NASA 2017 SnowEx Campaign and continues to work with the snow remote sensing community toward a snow satellite mission. He also serves as the NASA Instrument Scientist for the ATMS Microwave Sounder on the S-NPP and JPSS satellites.



Olivier Merlin received the Engineering degree in nuclear physics from the Ecole Nationale Supérieure de Physique de Grenoble, Grenoble, France, in 2000, the M.S. degree in techniques for space from the Ecole Nationale Supérieure de l'Aéronautique et de l'Espace, Toulouse, France, in 2001, and the Ph.D. degree in remote sensing and hydrology from the Universitat Sabatier, Toulouse, in 2005.

From 2006 to 2008, he was a Research Fellow with the University of Melbourne, Melbourne, VIC, Australia, where his work dealt with the mapping of surface and root-zone soil moisture at high spatial resolution. He joined CESBIO, Toulouse, in 2008, as a CNRS Researcher. His research includes land surface modeling and development of new (disaggregation, assimilation, and calibration) methods to facilitate the coupling between multisensor data and hydrologic models.



Valentijn R. N. Pauwels received the M.Sc.Eng. degree in agricultural sciences from Ghent University, Ghent, Belgium, in 1994, and the Ph.D. degree in civil engineering and operations research from Princeton University, Princeton, NJ, USA, in 1999.

From 1999 to 2004, he was a Post-Doctoral Research Fellow funded by the Foundation for Scientific Research of the Flemish Community. He undertook this position at Ghent University, where he joined as a Lecturer in 2005 and as a Senior Lecturer in 2010. In 2012, he joined Monash University, Clayton, VIC, Australia, where he is an Associate Professor. He is a Future Fellow funded by the Australian Research Council. His major research interests are hydrologic model development and optimization.



Luigi J. Renzullo (Member, IEEE) received the B.Sc. degree in mathematics and computing, the PostGrad.Dip. degree in applied physics, and the Ph.D. degree in remote sensing science from the Curtin University of Technology, Perth, WA, Australia, in 1996, 1997, and 2004, respectively.

In 2000, he joined Commonwealth Scientific and Industrial Research Organization (CSIRO) Mathematical and Information Sciences, North Ryde, NSW, Australia, as a Remote Sensing Analyst, where he worked on the radiometric processing and classification of sequences of Landsat TM and ETM+ imagery. In 2003, he was appointed as a Post-Doctoral Research Fellow with CSIRO Land and Water, Canberra, ACT, Australia, where he has been working on the analysis of reflectance spectrometry. His research interests include image processing and analysis, high-dimensional data mining, and regression.

Dr. Renzullo is a Graduate Member of the Australian Mathematical Society and a member of the Statistical Society of Australia.



Christoph Rüdiger (Senior Member, IEEE) received the B.E. degree in civil engineering from the RheinMain University of Applied Sciences, Wiesbaden, Germany, in 2002, and the Ph.D. degree in environmental engineering from the University of Melbourne, Melbourne, VIC, Australia, in 2008, with a focus on the potential to assimilate streamflow data into land surface models for soil moisture prediction.

In 2006, he joined the Centre National de Recherches Météorologiques, Météo France and also the French Space Agency (CNES), Toulouse, France, focusing on the performance analysis and data assimilation of land surface variables within the French land surface model ISBA in preparation of European Space Agency (ESA) SMOS mission. He returned to Australia in 2008 to coordinate and lead a number of Cal/Val campaigns for the Australian land validation segment of the SMOS mission in the Australian arid zone and the Murrumbidgee River catchment, and subsequently participated in the Cal/Val campaigns of SMAP. Since 2011, he has been a Faculty Member with the Department of Civil Engineering, Monash University, Clayton, VIC, where he has been the Director of Monash AgTech Launchpad since 2019, fostering interdisciplinary collaborations in this field. Since then, his research interests revolve around the remote sensing of vegetation and landscape water dynamics at high resolution for drought monitoring, wildfire predictions, and the development of EO applications in precision agriculture.



Sabah Sabaghy received the B.Eng. degree (Hons.) in water resources engineering from the University of Mazandaran, Babolsar, Iran, in 2010, the M.Sc. degree in geo-information science and Earth observation from the University of Twente, Enschede, The Netherlands, in 2013, and the Ph.D. degree in remote sensing and spatial data analysis from Monash University, Clayton, VIC, Australia, in 2019.

She is a Remote Sensing and Spatial Information Scientist with Agriculture Victoria Research Division, Victoria Government, Melbourne, VIC, Australia. Her research contributes to the application of remote sensing and spatial sciences for agricultural production and water resources management. Her Ph.D. thesis on harmonious downscaled soil moisture from passive microwave observations was within the framework of an Australian Research Council (ARC) Discovery Project. Her Ph.D. thesis was conducted in collaboration with NASA Goddard Space Flight Centre, Greenbelt, MD, USA; JPL, Pasadena, CA, USA; MIT, Cambridge, MA, USA; USRA, Columbia, MD, USA; USDA, Beltsville, MD, USA; CESBIO, Toulouse, France; the University of South California, Los Angeles, CA, USA; the Vrije University of Amsterdam, Amsterdam, The Netherlands; Max Planck Institute for Meteorology, Hamburg, Germany; and the University of Oxford, Oxford, U.K.



Christian von Hebel received the M.Sc. degrees in geophysics from TU Delft, ETH Zürich, and RWTH Aachen, in 2012, and the Ph.D. degree in hydrogeophysics from RWTH Aachen and Agrosphere Institute of Bio and Geosciences (IBG-3), Forschungszentrum Jülich, in 2016.

Until 2020, he held a post-doctoral position in hydro- and agrogeophysics at FZJ and Gembloux Agro-BioTech, respectively, and is currently working as the Soil Health Data Scientist at xarvio Digital Farming. His research interests include high-resolution soil sensing, soil and plant interaction, sustainable agriculture using variable rate applications, as well as developing new and novel sensors and data strategies for proximal soil sensing.



Simon H. Yueh (Fellow, IEEE) received the Ph.D. degree in electrical engineering from the Massachusetts Institute of Technology, Cambridge, MA, USA, in 1991.

In 1991, he joined Radar Science and Engineering Section, Jet Propulsion Laboratory (JPL), Pasadena, CA, USA, where he has assumed various engineering and science management responsibilities. He was a Project Scientist of the National Aeronautics and Space Administration (NASA) Aquarius mission from 2012 to 2013. He joined the NASA Soil Moisture Active Passive Mission, as the Deputy Project Scientist, in 2013, and has been the SMAP Project Scientist since 2013. He has been a Post-Doctoral Research Associate with the Massachusetts Institute of Technology since 1991. He has been the Principal or a Co-Investigator of numerous NASA and DOD research projects on remote sensing of ocean salinity, ocean wind, terrestrial snow, and soil moisture. He has authored four book chapters and published more than 200 publications and presentations.

Dr. Yueh is a member of the American Geophysical Union and the URSI Commission F. He received the 2014 IEEE GRSS Transaction Prize Paper Award, the 2010 IEEE GRSS Transaction Prize Paper Award, the 2002 IEEE GRSS Transaction Prize Paper Award, the 2000 Best Paper Award in the IEEE International Geoscience and Remote Symposium, the 1995 IEEE GRSS Transaction Prize Paper Award for an article on polarimetric radiometry, the JPL Lew Allen Award in 1998, the JPL Ed Stone Award in 2003, the NASA Exceptional Technology Achievement Award in 2014, and the NASA Outstanding Public Leadership Medal in 2017. He was an Associate Editor of the *Radio Science* from 2003 to 2007. He is the Editor-in-Chief of the IEEE TRANSACTIONS ON GEOSCIENCE AND REMOTE SENSING.



Liujun Zhu received the B.S. degree in geography from Zhejiang Normal University, Jinhua, China, in 2012, and the M.Sc. degree in geography information science from Nanjing University, Nanjing, China, in 2015. He is pursuing the Ph.D. degree in civil engineering with Monash University, Clayton, VIC, Australia.

From 2017 to 2018, he was a Visiting Ph.D. Student with the University of Michigan, Ann Arbor, MI, USA. His research interests include active microwave remote sensing, soil moisture retrieval, machine learning, and its applications in classification and change detection.